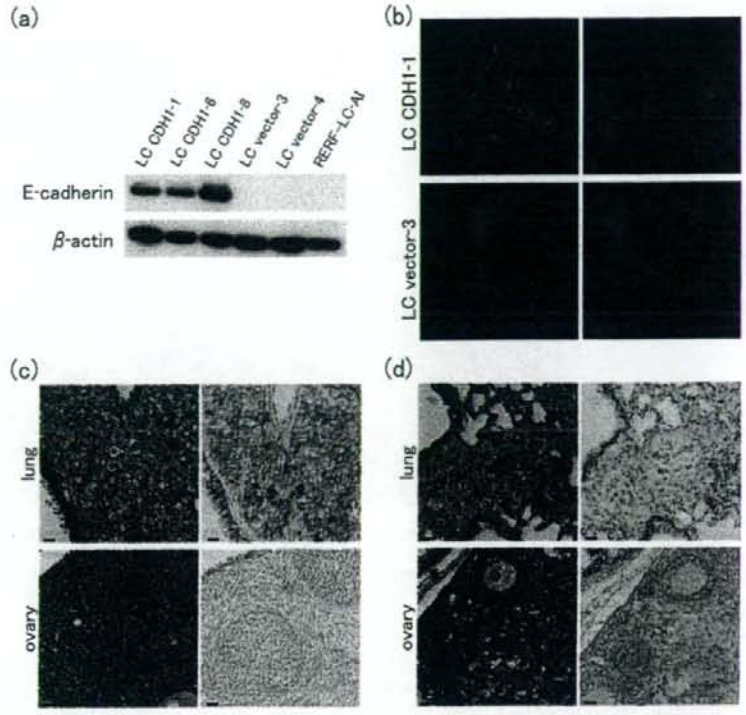

Fig. 3. Expression of E-cadherin in RERF-LC-AI transfectants (a,b) and representative findings of mouse tumors of the transfectants ([c] LC CDH-1 [d] LC vector-3). (a) Immunoblot analysis. E-cadherin transfectants were positive for E-cadherin, while mock clones and the parent cell line were negative. (b) Immunocytochemistry of LC CDH1-1, LC vector-3. Staining of E-cadherin (fluorescein-isothiocyanate–green), filamentous actin (phalloidin-red). LC CDH1-1 cells expressed E-cadherin, and merged staining of E-cadherin, actin, and nucleus (Hoechst-blue) showed membranous colocalization at the cell junction. (c,d) Hematoxylin–eosin staining and E-cadherin immunohistochemistry of the tumors. All clones tested showed tumorigenicity in the lung, and the lung tumors of E-cadherin transfectants showed E-cadherin expression in immunohistochemical staining. None of the E-cadherin transfectants metastasized to the ovary, while the mock clones showed high capacity for ovarian metastasis. Bar = 20 μm.

Table 5. Classification of clinical ovarian metastatic tumors by E-cadherin expression

Variables	E-cadherin expression		*P*-values
	Negative or weakly positive	Positive	
Number of cases	14	16	
Median age	48.6 (29–77)	59.2 (46–78)	0.014*
Primary organ			0.028**
Stomach	10	3	
Colon	2	13	
Breast	1	0	
Unclear	1	0	
Ovarian involvement			0.043*
Bilateral	11	8	
Unilateral	1	7	
Unclear	2	1	
Peritoneal dessemination			0.14
Positive	11	8	
Negative	3	8	
Histological findings of ovarian metastatic tumor			
Differentiation			0.00002**
Well or Moderate	0	12	
Poor	14	4	
Stromal proliferation			0.0002**
Positive	11	2	
Negative	3	14	

*$P < 0.05$; **$P < 0.01$.

transvenously and intraperitoneally. By clinical descriptions,[16,25,26] systemic circulation, peritoneal dissemination, and the lymphatic pathway are thought to be potential anatomical routes for metastasizing to the ovary. In our present model, hematogenous spread as well as the lymphatic pathway may be involved in the ovarian-specific metastasis by both transvenous and intraperitoneal inoculation. Transvenous inoculation of RERF-LC-AI and its transfectants of empty vector caused ovarian metastasis with remarkably high frequency, although the cells also metastasized to the other several organs. It could be considered that there

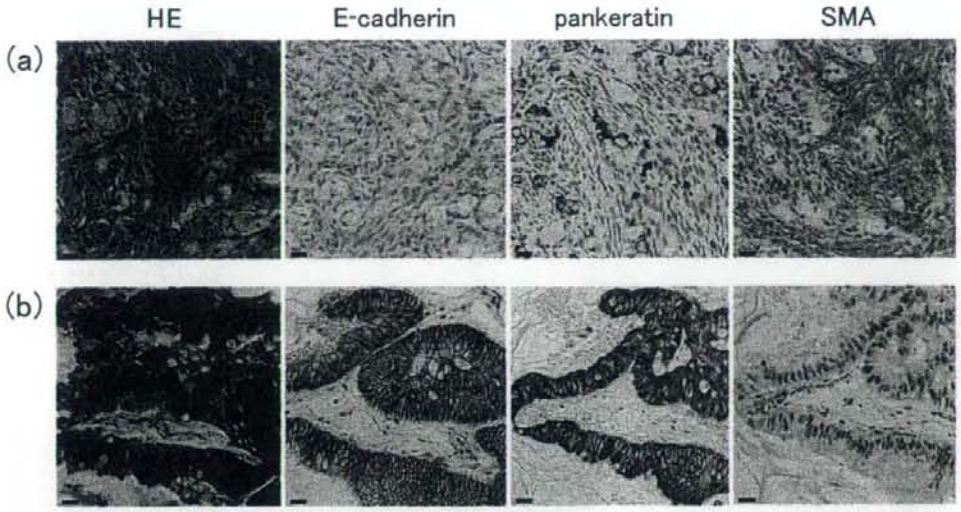

Fig. 4. Representative findings of ovarian metastatic tumors in clinical cases, hematoxylin–eosin (HE) and immunohistochemical staining. E-cadherin-negative or weakly positive case (a) and E-cadherin-positive case (b). HE staining and immunohistochemistry of E-cadherin, pankeratin (AE1/AE3), and smooth muscle actin (SMA). In (a), loss of E-cadherin expression and stromal proliferation were observed. In (b), metastatic tumor of well-differentiated adenocarcinoma showed E-cadherin positivity and relatively poor proliferation of stroma. Bar = 20 μm.

established an *in vivo* model of 'preferential' metastasis to the ovary, and then we utilized this model for investigation of molecular mechanisms of ovarian-specific metastasis.

Because all of the cell lines which metastasized to the ovary by intraperitoneal inoculation showed loss or reduction of E-cadherin expression on immunoblotting and/or immunohistochemistry, we hypothesized that E-cadherin down-regulation might be involved in the mechanism of ovarian-specific metastasis. To examine this hypothesis, RERF-LC-AI was transfected with the murine E-cadherin gene and inoculated into NOD/SCID mice transvenously. Forced expression of E-cadherin in RERF-LC-AI inhibited ovarian metastasis entirely and specifically, as it hardly affected metastasis to the other organs. E-cadherin is a transmembrane glycoprotein localized in the adherens junctions of epithelial cells and acts as a calcium-dependent adhesion molecule.[27] The reduction of E-cadherin expression increases mitotic activity of cancer cells, and promotes invasion and metastasis in general;[28,29] however, the results of our experiments indicate that loss or reduction of E-cadherin expression may promote, in particular, ovarian-specific metastasis. It has been shown that the germ line inactivating mutations in the E-cadherin gene causes hereditary diffuse gastric cancer syndrome, which is characterized by a high risk for diffuse gastric cancer and lobular breast cancer,[30,31] tumors that are associated with increased incidence of ovarian metastasis.[16,32] These data also support the hypothesis that E-cadherin down-regulation might be involved in ovarian-specific metastasis. Because it is hard to explain such involvement by only the function of E-cadherin as an adhesion molecule, there may be other unknown regulatory functions of E-cadherin, which can inhibit metastasis to the ovary.

Especially in organ-specific metastasis, the final step in metastatic events, where circulating cancer cells arrest and form tumor foci at distant sites, is considered to be an essential factor in specificity.[5,6] Those factors depend on the association of the characters of cancer cells and the microenvironment of the distant organ. For instance, osteoblastic bone metastasis of prostate carcinoma is closely associated with a series of biological interactions between tumor cells and bone cells where metastatic tumor cells release growth factors that in turn activate osteoblasts.[7] In classical Krukenberg tumor, ovarian stroma proliferates sarcomatously.[25,26] It can be hypothesized that there may be significant interaction between some types of cancer cells and ovarian stromal cells. Such tumor–stroma interaction may cause unique stromal proliferation and, perhaps as a result, help ovarian-specific metastasis. In our histological examination of clinical ovarian metastatic tumors, loss or reduction of E-cadherin expression was observed in about half of the cases. Interestingly, significant stromal proliferation and E-cadherin down-regulation emerged almost synchronously. Our *in vivo* model also demonstrated both E-cadherin down-regulation in RERF-LC-AI cells and stromal reaction in the ovary. Reduction of E-cadherin may be necessary for possible tumor–stroma interaction in ovarian-metastatic tumors.

In our clinical examination, most primary organs of E-cadherin down-regulated tumors were the stomach or breast, which are anatomically distant from the ovary. On the other hand, the majority of E-cadherin-positive tumors metastasized from the colon, which is relatively close to the ovary. This type of ovarian metastasis is considered to simply depend on anatomical proximity. Therefore, it is speculated that there are multiple types of metastasis to the ovary. The metastasis from relatively distant organs, which could be due to some propensity of cancer cells for ovarian metastasis and be regarded as ovarian-specific metastasis, may require E-cadherin down-regulation. In such type of metastasis, the interaction of carcinoma cells and ovarian stromal cells may help the metastasis.

In conclusion, we established an *in vivo* model of transvenous metastasis to the ovary. Our experiments using this model and investigation of clinical cases suggest the involvement of E-cadherin down-regulation in ovarian-specific metastasis.

Acknowledgments

This research was supported by a grant-in-aid from the 21th Century Center of Excellence (COE) program from the Ministry of Education, Culture, Sports, Science, and Technology of Japan, from the Third Term Comprehensive 10-Year Strategy for Cancer Control from the Ministry of Health, Labor, and Welfare of Japan, and from the Foundation for Promotion of Cancer Research. We are grateful to Tokiko Hirabayashi and Maki Morioka for the excellent technical support.

doi: 10.1111/j.1349-7006.2008.00946.x

References

1 Funasaka T, Raz A. The role of autocrine motility factor in tumor and tumor microenvironment. *Cancer Metast Rev* 2007; **26**: 725–35.
2 Fidler IJ. Critical determinants of metastasis. *Sem Cancer Biol* 2002; **12**: 89–96.
3 Fidler IJ. The organ microenvironment and cancer metastasis. *Differentiation* 2002; **70**: 498–505.
4 Strauli P, Haemmerli G. The role of cancer cell motility in invasion. *Cancer Metast Rev* 1984; **3**: 127–41.
5 Fokas E, Engenhart-Cabillic R, Daniilidis K, Rose F, An H-X. Metastasis: the seed and soil theory gains identity. *Cancer Metast Rev* 2007; **26**: 705–15.
6 Paget S. The distribution of secondary growths in cancer of the breast. *Lancet* 1889; **1**: 571–3.
7 Logothetis CJ, Lin SH. Osteoblasts in prostate cancer metastasis to bone. *Nat Rev Cancer* 2005; **5**: 21–8.
8 Cheng X, Hung MC. Breast cancer brain metastases. *Cancer Metastasis Rev* 2007; **26**: 635–43.
9 Young RH, Schully RE. Metastatic tumors in the ovary: a problem-oriented approach and review of the recent literature. *Semin Diagn Pathol* 1991; **8**: 250–76.
10 Urblight TM, Roth LM, Stehman FB. Secondary ovarian neoplasia: a clinicopathologic study of 35 cases. *Cancer* 1984; **53**: 1164–74.
11 Mazur MT, Hsueh S, Gersell DJ. Metastases to the female genital tract: analysis of 325 cases. *Cancer* 1984; **53**: 1978–84.
12 Fujiwara K, Ohishi Y, Koike H, Sawada S, Moriya T, Kohno I. Clinical implications of metastasis to the ovary. *Gynecol Oncol* 1995; **59**: 124–8.
13 Irving JA, Young RH. Lung carcinoma metastatic to the ovary: a clinicopathologic study of 32 cases emphasizing their morphologic spectrum and problems in differential diagnosis. *Am J Surg Pathol* 2005; **29**: 997–1005.
14 Fitzgibbons PL, Martin SE, Simmons TJ. Malignant melanoma metastatic to the ovary. *Am J Surg Pathol* 1987; **11**: 959–64.
15 Takenoue T, Yamada Y, Miyagawa S, Akiyama Y, Nagawa H. Krukenberg tumor from gastric mucosal carcinoma without lymphatic or venous invasion: report of a case. *Hepatogastroenterology* 2001; **48**: 1211–14.
16 Kakushima N, Kamoshida T, Hirai S *et al.* Early gastric cancer with Krukenberg tumor and review of cases of intramucosal gastric cancers with Krukenberg tumor. *J Gastroenterol* 2003; **38**: 1176–80.
17 Yakushiji M, Tazaki T, Nishimura H, Kato T. Krukenberg tumors of the ovary: a clinicopathologic analysis of 112 cases. *Acta Obst Gynaec Jpn* 1987; **39**: 479–85.
18 Wong PC, Ferenczy A, Fan L, McCaughey E. Krukenberg tumors of the ovary. Ultrastructual, histochemical, and immunohistochemical studies of 15 cases. *Cancer* 1986; **57**: 751–60.
19 Motoyama T, Hojo H, Watanabe H. Comparison of seven cell lines derived from human gastric carcinomas. *Acta Pathol Jpn* 1986; **36**: 65–83.
20 Ochiai A, Tahara E. Growth-promoting effect of gastrin on human gastric carcinoma cell line TMK-1. *Jpn J Cancer Res* 1985; **76**: 1064–71.
21 Ishiwata I, Ishiwata C, Soma M *et al.* Characterization of Krukenberg tumor cell line, especially the biological relationship between cancer and stromal cells. *Exp Pathol* 1990; **38**: 97–108.
22 Shimoyama Y, Hirohashi S, Hirano S *et al.* Cadherin cell-adheion molecules in human epithelial tissues and carcinomas. *Cancer Res* 1989; **49**: 2128–33.
23 Oda T, Kanai Y, Oyama T *et al.* E-cadherin gene mutations in human gastric carcinoma cell lines. *Proc Natl Acad Sci USA* 1994; **91**: 1858–62.
24 Yokozaki H. Molecular characteristic of eight gastric cancer cell lines established in Japan. *Pathol Int* 2000; **50**: 767–77.
25 Bidus MA, Zahn CM, Rose S. Germ cell, stromal, and other ovarian tumors. In: Disia P, Creasman W, eds. *Clinical Gynecologic Oncology*, 7th edn. Philadelphia: Mosby, 2007; 369–95.
26 Kim NK, Kim HK, Park BJ *et al.* Risk factors for ovarian metastasis following curative resection of gastric adenocarcinoma. *Cancer* 1999; **85**: 1490–9.
27 Yoshida-Noro C, Suzuki N, Takeichi M. Mollecular nature of the carcium-dependent cell–cell adhesion system in mouse teratocarcinoma and embryonic cells studied with a monoclonal antibody. *Dev Biol* 1984; **101**: 19–27.
28 Behrens J, Weidner KM, Frixen UH *et al.* The role of E-cadhein and scatter factor in tumor invasion and cell motility. *EXS* 1991; **59**: 109–26.
29 Takeichi M. Cadherins in cancer: implications for invasion and metastasis. *Curr Opin Cell Biol* 1993; **5**: 806–11.
30 Graziano F, Humar B, Guilford P. The role of E-cadherin gene (*CDH1*) in diffuse gastric cancer susceptibility: from the laboratory to clinical practice. *Ann Oncol* 2003; **14**: 1705–13.
31 Pharoah PD, Guilford P, Caldas C. Incidence of gastric cancer and breast cancer in *CDH1* (E-cadherin) mutation carriers from hereditary diffuse gastric cancer families. *Gastroenterology* 2001; **121**: 1348–53.
32 Harris M, Howell A, Chrissohou M, Swindell RI, Hudson M, Sellwood RA. A comparison of the metastatic pattern of infiltrating lobular carcinoma and infiltrating ductal carcinoma of the breast. *Br J Cancer* 1984; **50**: 23–30.

The American Journal of Pathology, Vol. 173, No. 4, October 2008

DOI: 10.2353/ajpath.2008.070309

Tumorigenesis and Neoplastic Progression

Reconstitution of Schwannian Stroma in Neuroblastomas Using Human Bone Marrow Stromal Cells

Wenlin Du,* Nobumichi Hozumi,† Michiie Sakamoto,* Jun-ichi Hata,*‡ and Taketo Yamada*

From the Department of Pathology, Keio University School of Medicine, Tokyo; the Institute for Biological Sciences,† Science University of Tokyo, Noda City; and the National Center for Child Health and Development,‡ Tokyo, Japan*

The Schwannian stroma in neuroblastomas is related to patient prognosis. There is debate surrounding the origin of Schwannian stroma in neuroblastomas: one theory is that the Schwann cells are derived from neoplastic cells, and the other is that they arise from normal cells surrounding the neuroblastoma. We examined whether human bone marrow stromal cells (hBMSCs) or human mesenchymal stem cells (hMSCs) could differentiate into Schwann cells in neuroblastomas. hBMSCs or hMSCs along with enhanced green fluorescent protein (EGFP) were injected into xenotransplanted neuroblastomas in nonobese diabetic mice with severe combined immunodeficiency and the resulting tumors were analyzed using immunohistochemistry. HBMSCs and hMSCs were co-cultured with neuroblastoma cells, and the induction of Schwann cell-specific molecules, S100beta and Egr-2, was monitored. S100beta-positive Schwannian stroma was observed only in neuroblastomas containing either hBMSCs or hMSCs, but not in neuroblastomas lacking these cells. Double staining with anti-S100 and anti-EGFP antibodies showed that S100-positive cells in neuroblastomas were also EGFP-positive. By contrast, hBMSCs did not develop into Schwann cells in Ewing's sarcoma, demonstrating that differentiation of transplanted hBMSCs or hMSCs into Schwann cells occurs specifically in neuroblastomas. Both S100beta and Egr-2 were expressed in hBMSCs or hMSCs co-cultured with neuroblastoma cells. HBMSCs or hMSCs may contribute to the formation of human tumor stroma. The Schwannian stroma of neuroblastomas appears to be derived from nonneoplastic stromal cells rather than neuroblastoma cells, further clarifying its developmental origins. *(Am J Pathol 2008, 173:1153–1164; DOI: 10.2353/ajpath.2008.070309)*

Neuroblastoma (NB) is an embryonal neoplasm that develops in the peripheral sympathetic nervous system and is derived from neural crest cells. It is the most frequently diagnosed neoplasm in children under 4 years of age. Neuroblastic tumors consist of two cell populations: neuroblastic/ganglionic cells and Schwann cells. Based on the maturation sequence of the neuroblastic cells and the volume of the Schwannian stroma, neuroblastic tumors have been morphologically classified into four categories by the International Neuroblastoma Pathology Committee: neuroblastoma (Schwannian stroma-poor); ganglioneuroblastoma, intermixed (Schwannian stroma-rich); ganglioneuroma (Schwannian stroma-dominant); and ganglioneuroblastoma, nodular (composites of Schwannian stroma-rich/stroma-dominant and stroma-poor components).[1,2] The prognosis of patients with NB is based on the volume of the Schwannian stroma, the degree of tumor cell differentiation, the number of tumor cell mitoses, and karyorrhexis.[1–4] The existence and development of Schwannian stroma is important for the prognosis of patients with NB.

The origin of the Schwannian stromal cell is controversial, and the relationship between Schwannian stromal cells and neuroblastic cells has not yet been clarified. One hypothesis is that both the Schwannian stromal cells and the neuroblastic cells arise from pluripotent neoplastic cells originating from the neural crest. Mora and col-

Supported by the Program for Promotion of Fundamental Studies in Health Sciences of the National Institute of Biomedical Innovation (07-17), Grants-in Aid for Pediatric Research (9C-5, 12C-1) from the Ministry of Education in Japan (05-045-0203), and Keio Gijuku Academic Development Funds and a special grant-in-aid for innovative and collaborative research projects at Keio University.

Accepted for publication July 8, 2008.

Supplemental material for this article can be found on http://ajp.amjpathol.org.

Address reprint requests to Taketo Yamada, M.D., Department of Pathology, Keio University School of Medicine, 35 Shinanomachi, Shinjuku-ku, Tokyo 160-8582, Japan. E-mail: taketo@sc.itc.keio.ac.jp.

leagues[5] showed that Schwann cells have the same genetic features as neuroblastic cells. An alternative theory, proposed by Ambros and colleagues[6,7] and Katsetos and colleagues[8] stated that the Schwann cells in neuroblastic tumors are likely to be reactive in nature and may have been recruited from nonneoplastic tissues surrounding the tumor cells. Ambros and colleagues[9] also reported that the Schwann cells induced NB cell neural differentiation and apoptosis *in vitro*. As yet, there is little research on the interaction between NB cells and Schwann cells. We have examined whether NB cells can induce the differentiation of bone marrow stromal cells or mesenchymal stem cells into Schwann cells.

Tumor stroma is indispensable for tumor development. Cell growth, apoptosis, motility, and the invasiveness of the cancer cells are all critically influenced by stroma-tumor interactions. Human bone marrow stromal cells (hBMSCs) are multipotential and can differentiate into tissues such as endothelium, muscle, myofibroblast, and neural cells.[10] Recently, some reports showed that bone marrow cells constitute part of tumor vessels and fibrous stroma.[11–13] Animal models have been developed for *in vivo* research on tumor stroma,[13,14] however, these models, using rodent stroma, may not be appropriate for examining the biological function of human tumor stroma. Here, we examined whether hBMSCs are capable of forming tumor stroma by inoculating hBMSCs into xenografted tumors in NOD/SCID mice.

The Schwannian stroma in NB tumors is a very specific stroma compared with other tumor stroma concerning differentiation and prognosis of NB tumors. We examined whether nonneoplastic cells (hBMSCs or human fibroblasts) could differentiate into Schwann cells in NB tumors. We conducted *in vivo* experiments in which hBMSCs or human fibroblasts were inoculated into xenotransplanted NBs in NOD/SCID mice and the tumor stroma analyzed using immunohistochemistry. The ability of hBMSCs or human fibroblasts to differentiate into Schwann cells through co-culture with NB cells was also examined.

Materials and Methods

Isolation and Culture of Primary hBMSCs

Bone marrow was aspirated from the costa or sternum of patients with lung neoplasms or pectus excavatum, and suspended in Iscove's modified Dulbecco's medium. Mononucleated cells, including stromal cells, were isolated by centrifugation for 30 minutes at 400 × *g* (room temperature) using Lymphosepar (IBL, Fujioka, Japan), washed twice in Iscove's modified Dulbecco's medium, and seeded in a 10-cm dish containing Iscove's modified Dulbecco's medium with 10^{-6} mol/L hydrocortisone, 10^{-4} mol/L 2-mercaptoethanol (Sigma-Aldrich, Sheinheim, Germany), 100 IU/ml penicillin, 100 μg/ml streptomycin, 15% heat-inactivated fetal bovine serum, and 12.5% heat-inactivated horse serum (Moregate BioTech, Bulimba, Australia). The hBMSCs adhered 1 day after bone marrow isolation and were expanded for 3 to 4 days. After the nonadherent cells were decanted, the adherent stromal layer was trypsinized and transferred to two 10-cm plates. Flow cytometry showed that the hBMSCs were $CD13^+$, $CD29^+$, $CD44^+$, $CD106^+$, $CD166^+$, $CD14^-$, $CD31^-$, $CD34^-$, $CD43^-$, $CD45^-$, $CD71^-$, $CD105^-$, and $S100beta^-$. All human material was used with the approval (approval numbers 13-1 and 12-1) of the Ethics Committee of Keio University School of Medicine and with the signed, informed consent of patients.

Cell Lines and Culture Conditions

Human mesenchymal stem cells (hMSCs; Osiris Therapeutics Inc., Columbia, MD) were cultured using the human mesenchymal stem cell bullet kit (BioWhittaker, Inc., Walkersville, MD). HMSCs have been reported to differentiate into osteogenic, chondrogenic and adipogenic lineages. Flow cytometry showed that the hMSCs were $CD29^+$, $CD44^+$, $CD105^+$, $CD106^+$, $CD166^+$, $CD14^-$, $CD31^-$, $CD34^-$, $CD43^-$, $CD45^-$, and $S100beta^-$.[15] The NB cell lines SK-N-DZ and SK-N-AS (CRL-2149 and CRL-2137; American Type Culture Collection, Rockville, MD) were cultured in Dulbecco's modified Eagle's medium with 100 IU/ml penicillin, 100 μg/ml streptomycin, and 10% heat-inactivated fetal bovine serum (JRH Biosciences, Lenexa, KS).SK-N-DZ cells are derived from a poorly differentiated embryonal NB and exhibit MYCN amplification (30 times). Retinoic acid induces differentiation of the SK-N-DZ cells.[16] SK-N-AS cells are derived from a poorly differentiated embryonal NB and do not exhibit MYCN amplification. Retinoic acid partially inhibits proliferation, and SK-N-AS cells fail to differentiate after retinoic acid treatment.[17] The Ewing's sarcoma cell line RD-ES (HTB-116, American Type Culture Collection) was cultured in RPMI 1640 medium with 100 IU/ml penicillin, 100 μg/ml streptomycin, and 10% heat-inactivated fetal bovine serum. The human fibroblast cell lines MRC-5 (CCL-171, American Type Culture Collection), KMS-6 (JCRB0432; Health Science Research Resources Bank, Osaka, Japan), and HE-1 (IFO050297, Health Science Research Resources Bank) were cultured in minimum essential medium Eagle with 100 IU/ml penicillin, 100 μg/ml streptomycin, and 10% heat-inactivated fetal bovine serum. All cells, including the primary hBMSCs, were grown at 37°C in the presence of 95% humidity and 5% CO_2.

Retroviral Vector and Its Producer Cells

The enhanced green fluorescent protein (EGFP) retroviral vector and the amphotropic producer cells, PG13/MSGFP, were provided by Dr. Robert G. Hawley of the American Red Cross, Washington, DC. The retroviral vector was constructed to contain only the 5′ and 3′ long terminal repeat promoter (LTR) and EGFP gene, and not the neomycin gene. The PG13/MSGFP producer cells were cultured in Dulbecco's modified Eagle's medium containing 4.5 g/L glucose plus 10% fetal bovine serum. The supernatant of the PG13/MSGFP cells was used for the retroviral transductions of the hBMSCs and hMSCs.

Transduction of Bone Marrow Stromal Cells

HBMSCs or hMSCs were seeded in a 10-cm dish. When the cells reached 80% confluence, the supernatant was discarded and 5 ml of a viral solution containing 2.5 ml of the supernatant of amphotropic producer cells (PG13/MSGFP), an equal volume of media for the primary hBMSCs or hMSCs, and 4 μg/ml of polybrene (Sigma, St. Louis, MO), were added. The cells were then incubated for 2 hours. Four rounds of transductions were performed, and 5 ml of fresh media was added after the last round of transduction. After 24 hours, the supernatant of the stromal cells was changed with fresh media. The cells were transduced with EGFP-retroviral vector and allowed to expand for1 week; the presence of EGFP-positive cells was detected using flow cytometry.

Transplantation of NB Cells and hBMSCs or hMSCs in NOD/SCID Mice

NOD/SCID mice were maintained under specific, pathogen-free conditions and used at 6 to 10 weeks of age. All experimental procedures and protocols were approved by the Animal Ethics Committee of the Keio University School of Medicine. NB cells, SK-N-DZ or SK-N-AS, were suspended (1×10^7 cells) in 100 μl of Dulbecco's modified Eagle's medium and transplanted subcutaneously into the NOD/SCID mice. Two weeks after transplantation, hBMSCs or hMSCs containing the EGFP-retroviral vector (3×10^6 cells) in 50 μl of Iscove's modified Dulbecco's medium were inoculated into the subcutaneous NB tumors of the NOD/SCID mice. NB tumors inoculated with media only served as negative controls. The NB tumors inoculated with or without hBMSCs or hMSCs were excised 9 days after inoculation and processed for histological examination. The process was repeated using Ewing's sarcoma cells RD-ES (1×10^7 cells) transplanted subcutaneously into NOD/SCID mice and the subcutaneous Ewing's sarcoma inoculated with hBMSCs.

Examination of EGFP-Positive Cells

The subcutaneous NB tumors from the NOD/SCID mice were cut in half and fixed in 4% paraformaldehyde for 24 hours. One half of each tumor was embedded in paraffin for histological examination and immunohistochemistry. The other half was frozen in Tissue-Tec OCT (Sakura, Tokyo, Japan) in isopentane with dry ice. Cryosections (6 to 8 μm) were fixed in 4% paraformaldehyde for 5 minutes. EGFP-fluorescence was observed using a confocal laser microscope (LSM510; Carl Zeiss, Tokyo, Japan) with a 488-nm laser and a 505- to 530-nm bandpass filter.

Immunohistochemistry and Immunocytochemistry

The paraffin-embedded xenografted NB tumor sections were stained with a mouse monoclonal GFP antibody (1:2000; MBL, Nagoya, Japan), using an indirect immunohistochemical technique to identify the EGFP-positive cells. The Schwann cells in the NBs were stained with an anti-S100 polyclonal antibody (1:1000; DakoCytomation, Glostrup, Denmark), a S100beta monoclonal antibody (1:100; Santa Cruz Biotechnology, Santa Cruz, CA), and a human NGFRp75 monoclonal antibody (1:200, Santa Cruz Biotechnology). The stromal components of the NBs were stained with an α-smooth muscle actin monoclonal antibody (1:200, DakoCytomation). Immunohistochemistry for Egr-2 was performed on cryosections of NB tumors from patients with an Egr-2 rabbit polyclonal antibody (1:400, Santa Cruz Biotechnology). Antigen retrieval was performed with 10 mmol/L citrate buffer (pH 6.0) for S100beta and α-smooth muscle actin, heated in a boiling steamer for 10 minutes, and cooled down to room temperature for 20 minutes. For S100, GFP, and human NGFRp75, antigen retrieval was performed with 0.1% trypsin (Difco Laboratories, Detroit, MI) at room temperature for 30 minutes. All sections were blocked with 2.5% normal horse serum for 30 minutes at room temperature and incubated with the primary antibodies in a humidity chamber overnight at 4°C, and visualized with diaminobenzidine (ImmPress Reagen kit; Vector Laboratories, Burlingame, CA). The sections were immunohistochemically dual-stained for EGFP-positive and S100-positive cells using alkaline phosphatase with Fast blue BB (for the mouse anti-GFP antibody), and horseradish peroxidase with diaminobenzidine (for the anti-S100 antibody). The sections were also immunohistochemically dual-stained for EGFP-positive and α-smooth muscle actin-positive cells using alkaline phosphatase with Fast blue BB (for the mouse anti-GFP antibody), and horseradish peroxidase with diaminobenzidine (for the α-smooth muscle actin antibody).

Immunofluorescence Observations

Cryosections of xenografted NB tumor were processed for dual-immunofluorescence staining of EGFP-positive/S100-positive and EGFP-positive/Egr2-positive cells. EGFP-positive cells were stained with a mouse monoclonal GFP antibody (1:2000) and a secondary goat anti-mouse Cy3-conjugated antibody (1:100; Jackson ImmunoResearch Laboratories, West Grove, PA). S100-positive cells were stained with a S100 polyclonal antibody (1:1000) and a secondary goat anti-rabbit Cy5-conjugated antibody (1:100, Jackson ImmunoResearch Laboratories). Egr-2-positive cells were stained with an Egr-2 rabbit polyclonal antibody (1:200) and a secondary goat anti-rabbit Cy5-conjugated antibody (1:100). All sections were blocked with 5% normal goat serum before incubation with primary antibodies. Digital images were obtained using a Zeiss confocal laser microscope (LSM510) with a 543-, 633-nm laser and a 560-, 650-nm bandpass filter.

Co-Culture of hBMSCs or hMSCs and NB Cells

The hBMSCs, hMSCs, or human fibroblasts were trypsinized and placed on six-well plates for transwells

(pore size, 0.4 μm; Corning Costar, Cambridge, MA) at a density of 2×10^4 stromal cells/well. The transwells were inserted and 1×10^5 NB cells, either SK-N-DZ or SK-N-AS in a suspension of Dulbecco's modified Eagle's medium containing 10% fetal bovine serum, were added to each transwell. The hBMSCs were also co-cultured in contact with NB cells, in the same wells of the six-well plates, at a density of 1×10^4 stromal cells, and 1×10^4 NB cells/well. Every 3 days the cultures were refreshed with an equal volume of Dulbecco's modified Eagle's medium for the NB cells and media for the stromal cells or fibroblasts. A proportion of the wells were treated with 1 μg/ml of transforming growth factor-β (TGF-β), 5 μg/ml glial-derived neurotrophic factor (GDNF), 25 μg/ml sensory and mortar neuron-derived factor (SMDF), 20 μg/ml 3,3,5-triiodo-L-thyonine sodium salt (T3), 1 mg/ml L-throxine sodium salt pentahydrate T4, 0.5 mmol/L forskolin, and 10 μg/ml of nerve growth factor (NGF) to examine the induction of Schwann cell differentiation by the hBMSCs or fibroblasts.[18–22] Before co-culture, hBMSCs were labeled using a fluorescent cell linker kit (PKH26-GL, PKH67-GL; Sigma-Aldrich Co., Vienna, Austria) following the instructions of the manufacturer.

Quantification of S100beta Induction

After1 week of culture, the hBMSCs labeled with the green fluorescent cell linker kit (PKH67-GL) were stained with aS100beta monoclonal antibody and a secondary goat anti-mouse Cy3-conjugated antibody, and mounted with mounting medium with 4,6-diamidino-2-phenylindole (DAPI) (Vector Laboratories). Digital images were obtained using a confocal laser microscope (LSM510; Carl Zeiss) with a 405-, 488-, 543-nm laser and a 420-, 505-, 560-nm bandpass filter. S100beta-positive hBMSCs, after co-culture with NB cells, were quantified by the ArrayScan V^{T1} system (Cellomics, Pittsburgh, PA). The hBMSCs labeled with the red fluorescent cell linker kit (PKJ26-GL) were stained with aS100beta monoclonal antibody and a secondary rabbit anti-mouse fluorescein isothiocyanate (FITC) antibody (DakoCytomation). The nuclei were stained with Hoechst 33342. Images were captured by the Cellomics ArrayScan V^{T1} from a total of 50 fields (1 field = 660 μm × 660 μm) per well using three separate fluorescent filters at ×10 objective magnification. Channel 1 (blue, 365 nm × 50 nm bandwidth filter) excites Hoechst 33342, channel 2 (green, 475 nm × 40 nm bandwidth filter) excites objects stained with FITC-labeled S100beta, and channel 3 (red, 575 nm × 25 nm bandwidth filter) excites PKH26. Morphometry was analyzed using the Target Activation BioApplication assay protocol (Cellomics). The Target Activation Bioapplication reports the fluorescent intensities of each object in the field, based on user-defined fluorescent intensity thresholds set in the blue, green, and red images. This application also reports the number of cells that were defined as an object/cell with both green and red fluorescent intensity values, inside a range defined by the user. The percentage of S100beta-FITC-positive hBMSCs from the total of hBMSCs labeled with red fluorescent linker PKH26-GL, is reported.

Flow Cytometry Analysis of NB Cells after Co-Culture with hBMSCs or hMSCs

The SK-N-DZ cells and SK-N-AS cells were stained with a ssDNA rabbit polyclonal antibody (1:200, DakoCytomation) and a secondary swine anti-rabbit FITC-conjugated antibody (1:100, DakoCytomation), after co-culture with hBMSCs or hMSCs, to identify apoptosis of the NB cells. The NB cells were also stained with a MIB-1 mouse monoclonal antibody (1:100, DakoCytomation) and a secondary rabbit anti-mouse FITC-conjugated antibody (1:100, DakoCytomation) after co-culture to analyze cell proliferation.

Immunoblotting

HBMSCs or fibroblasts in six-well plates were washed with phosphate-buffered saline, dissolved in RIPA buffer containing 1 mmol/L ethylenediaminetetraacetic acid, 0.1% sodium dodecyl sulfate, 1% IGEPAL, 150 mmol/L NaCl, 10 mmol/L Tris, and 10 μg/ml aprotinin (Sigma), and centrifuged (15,000 rpm, 15 minutes, 4°C). The supernatant of the cell lysates was transferred to a new tube. The protein concentrations were determined using a standard bovine serum albumin curve (DC Protein Assay Kit II; Bio-Rad, Hercules, CA). Equal amounts of protein were subjected to sodium dodecyl sulfate-polyacrylamide gel electrophoresis using NuPAGE 4 to 12% Bis-Tris gel (Invitrogen, Carlsbad, CA) and blotted onto a polyvinylidene difluoride membrane. The membrane was blocked with 5% skim milk (Becton Dickinson, Franklin Lakes, NJ) in Tris-buffered saline containing Tween 20 (Sigma-Aldrich) (TBS-T). Egr-2 or HSC70 was detected using enhanced chemiluminescence (ECL; Amersham, Buckinghamshire, UK) and primary antibodies against human Egr-2 (rabbit polyclonal IgG, diluted 1:1000; Santa Cruz Biotechnology) or human HSC70 (mouse monoclonal IgG, diluted 1:1000; Santa Cruz Biotechnology) and horseradish peroxidase-conjugated secondary antibody (goat anti-rabbit IgG-HRP, diluted 1:1000; Santa Cruz Biotechnology).

Results

hBMSCs and hMSCs

The primary hBMSCs were spindle-shaped and grew constantly (Figure 1A1). A proportion of the hBMSCs differentiated into endothelial cells, as shown by the uptake of Dil-Ac-LDL on day 10 (Figure 1A2). On day 30, numerous lipid droplets in the cytoplasm of the hBMSCs and red-colored droplets were observed when the cells were examined using oil red O stain (Figure 1A, 3 and 4). The primary hBMSCs were harvested from human bone marrow and transduced with an EGFP-retroviral vector. More than 70% of the primary hBMSCs were EGFP-positive on day 9 after transduction (Figure 1B). Sixty to seventy percent of the hMSC cell line were EGFP-positive after the retroviral transduction

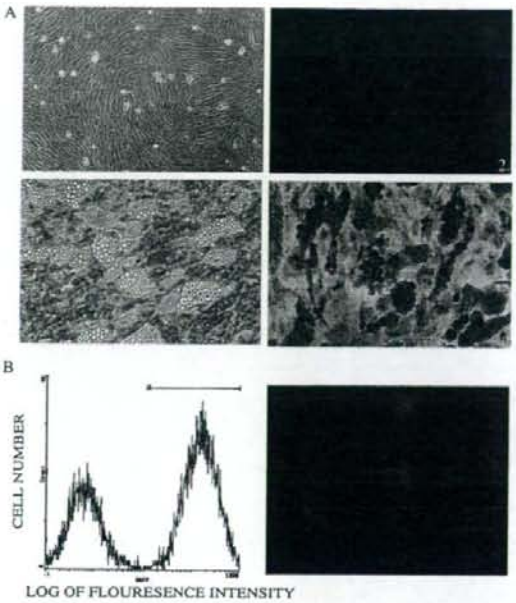

Figure 1. hBMSCs and gene transfer with EGFP-retroviral vector into hBMSCs. **A:** Phenotype of the hBMSCs. **1:** The hBMSCs harvested from human bone marrow tissues were elongated and spindle-shaped (phase-contrast microscopy). **2:** Uptake of Dil-Ac-LDL on day 10 (fluorescence microscopy). **3:** Numerous lipid droplets in the cytoplasm of hBMSCs on day 30 (phase contrast microscopy). **4:** Red-colored lipid droplets were shown by staining with oil red O. **B:** hBMSCs transduced with the EGFP retroviral vector. Primary cultured hBMSCs were transduced with an EGFP retroviral vector. More than 70% of the primary hBMSCs were EGFP-positive on day 9 after the transduction. The figure on the **left** shows EGFP positivity by flow cytometry and the figure to the **right** shows EGFP positivity by confocal laser microscopy. Original magnifications, ×120.

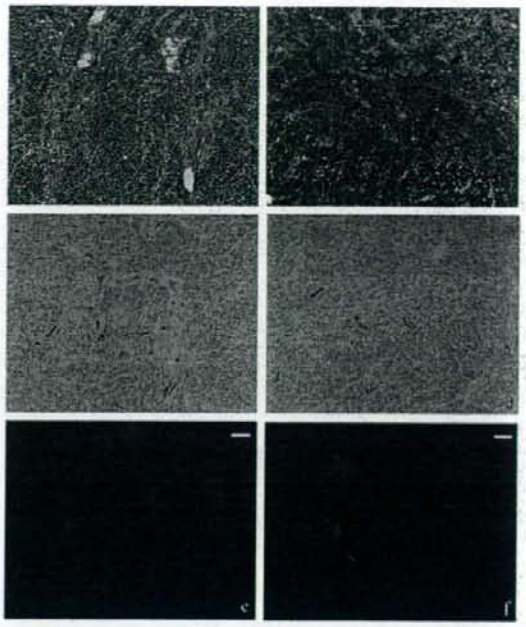

Figure 2. hBMSCs inoculated into NB tumors in nonobese diabetic mice with severe combined immunodeficiency (NOD/SCID) mice. The hBMSCs with EGFP expression were inoculated in the xenografts of two lines of NB cells, SK-N-DZ (**a**, **c**, and **e**) and SK-N-AS (**b**, **d**, and **f**).These NB tumors contained stromal components that produced an irregular net-like formation (**a** and **b:** H&E stain). EGFP-positive hBMSCs were distributed diffusely in the tumor stroma (**c** and **d:** immunohistochemistry with anti-EGFP antibody). EGFP-positive hBMSCs were confirmed with green fluorescence using a confocal laser microscope (**e** and **f**). Scale bars = 50 μm.

(Supplemental Figure S1, see *http://ajp.amjpathol.org*). The flow cytometry results of S100beta$^-$ in hBMSCs and hMSCs did not change after transduction.

Transplantation of Human NB Cells and Human Stromal Cells

The NB cells, SK-N-DZ or SK-N-AS, were transplanted subcutaneously into NOD/SCID mice. After 2 weeks, tumors with diameters of 5 mm were observed in the subcutaneous tissues. Primary hBMSCs transduced with the EGFP-retroviral vector were inoculated into the NB tumors. Figure 2, a and b, shows NB tumors (SK-N-DZ and SK-N-AS, respectively) with stromal components exhibiting an irregular net-like formation. The distribution of EGFP-positive cells was diffuse among the stromal components of the NB tumors (Figure 2, c and d; SK-N-DZ and SK-N-AS, respectively). Green-fluorescent cells in the frozen NB tumor sections (SK-N-DZ and SK-N-AS) were observed using a confocal laser microscope (Figure 2, e and f, respectively). These results show that the hBMSCs inoculated into the NB tumors survived and constituted a portion of the tumor stroma. Reconstitution of the tumor stroma using hMSCs was also seen (Supplemental Figure S2, see *http://ajp.amjpathol.org*).

Schwannian Differentiation of hBMSCs in NBs

Schwann cells in the xenografted NB tumors were detected using a S100 polyclonal antibody, which reacted with both human and murine S100 proteins, similar to the method used for the pathological diagnosis of NB tumors. S100-positive cells were not observed in the NB tumors (SK-N-DZ) that were not inoculated with hBMSCs (Figure 3h). We examined the expression of S100beta, Schwann cell-specific molecules, and human NGFRp75 using immunostaining. S100beta- and p75-positive cells were detected in the xenografted NB tumors inoculated with hBMSCs (Figure 3, b and c), but were not detected in the NB tumors without the inoculation of hBMSCs (Supplemental Figure S3A, i and j; see *http://ajp.amjpathol.org*). Tumor stroma with S100-, S100beta-, and p75-positive cells was also observed in SK-N-AS tumors injected with hBMSCs (Supplemental Figure S3A, b–d; see *http://ajp.amjpathol.org*). These results show that Schwannian stroma derived from murine cells was not induced in the human NB tumors. On the other hand, S100/S100beta-positive cells were observed in the irregular net-like stroma of NB tumors (SK-N-DZ) inoculated with hBMSCs (Figure 3, a and b). These S100/S100beta-positive cells were spindle-shaped and found among the stromal components (Figure 3, a and b). We examined whether these S100-positive cells originated from the inoculated EGFP-

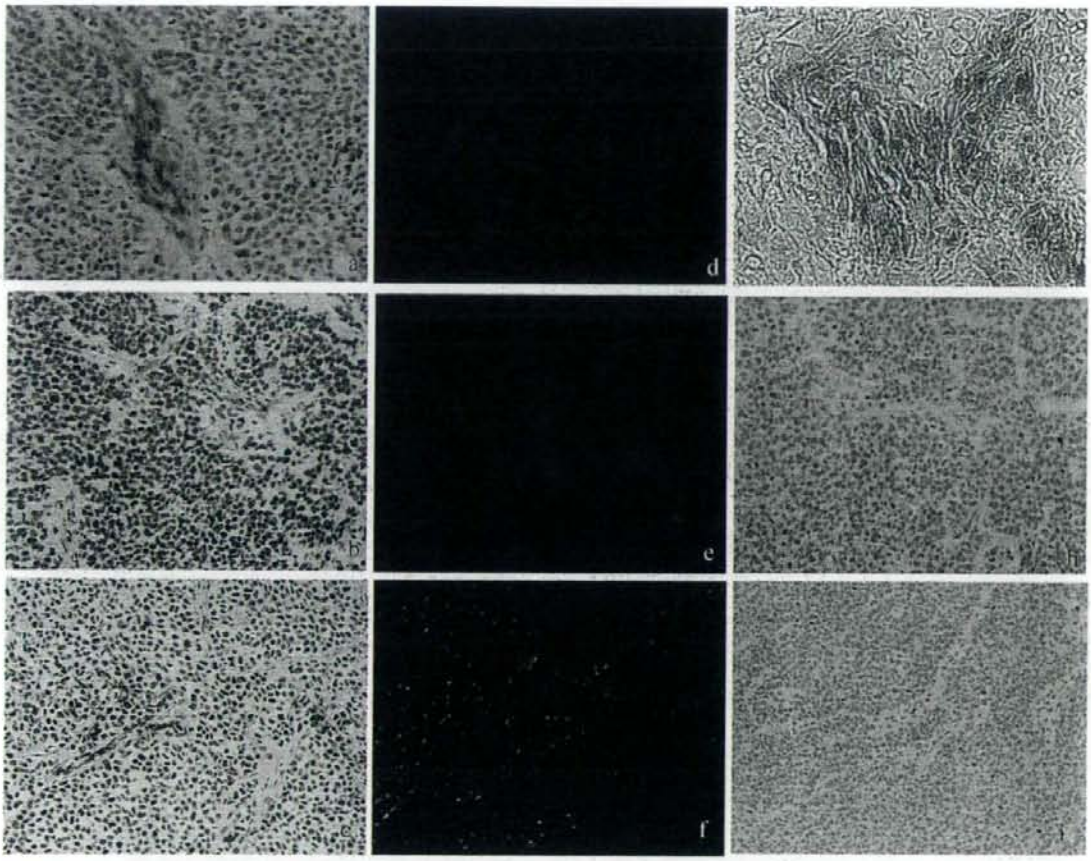

Figure 3. Schwannian differentiation of hBMSCs in NB. Schwann cells in the xenografted NB tumor were detected by immunohistochemistry and immunofluorescence using a S100 polyclonal antibody, aS100beta monoclonal antibody, and a human NGFRp75 monoclonal antibody. **a:** S100-positive cells were observed in the irregular net-like stroma of NB tumor (SK-N-DZ) inoculated with hBMSCs. These S100-positive cells were spindle-shaped and existed in stromal components. **b:** Schwann cells positive for the specific marker S100beta were detected in the stroma of NB tumors (SK-N-DZ cells). **c:** Human NGFRp75-positive cells were observed in the stroma of NB tumors (SK-N-DZ cells). **d**, **e**, and **f:** Immunofluorescent dual-staining with EGFP (**d**; using secondary Cy3-conjugated antibody, red) and S100 (**e**; using secondary Cy5-conjugated antibody, blue). S100-positive cells (**e**) were also positive for EGFP (**d**, **f**). **g:** S100-positive cells (brown) were almost always positive for EGFP (blue). These S100-positive cells may have originated from inoculated EGFP-hBMSCs. **h:** S100-positive cells were not observed in the NB tumors (SK-N-DZ) without the inoculation of hBMSCs. **i:** Human Ewing's sarcoma cells (RD-ES) were transplanted in NOD/SCID mice subcutaneously and then hBMSCs were inoculated into the Ewing's sarcoma tumors. There were no S100beta-positive cells in the Ewing's sarcoma tumors.

hBMSCs using immunohistochemical or immunofluorescent double-staining for S100 and EGFP. We found the S100-positive cells were similarly almost always positive for EGFP (Figure 3, d–g). The induction of S100-positive stromal cells in SK-N-AS cell-derived NB tumors inoculated with hBMSCs was also observed (Supplemental Figure S3A, e–h, see *http://ajp.amjpathol.org*). These results suggest that the S100-positive Schwann cells were derived from the inoculated hBMSCs.

We also examined whether the induction of Schwann cells from hBMSCs could be observed in human carcinomas other than NBs. Human Ewing's sarcoma cells (RD-ES) were transplanted into NOD/SCID mice subcutaneously and the resulting Ewing's sarcoma tumors were inoculated with hBMSCs. EGFP-positive stromal cells were seen in the Ewing's sarcoma tumors as well as in the NB tumors (Supplemental Figure S3A, k and l; see *http://ajp.amjpathol.org*). However, S100beta-positive Schwann cells were not observed in the Ewing's sarcoma tumors (Figure 3i). The induction of S100/S100beta/p75-positive stromal cells in NB tumors inoculated with hMSCs was also seen (data not shown). These results suggest that hBMSCs or hMSCs constitute human stromal components *in vivo* and differentiate into S100-positive Schwannian stroma only when in NBs similar to clinical NB tumors.

We also examined the expression of Egr-2, a transcription factor expressed during the early development of Schwann cells, in NB tumors.[23] In differentiating NB tumors from patients, a small number of Egr2-positive cells were observed in the stroma of differentiating NB tumors (Figure 4, a and b). In xenografted NB tumors, Egr-2-positive cells were detected in the stroma, and most of these Egr-2-positive cells were also EGFP-

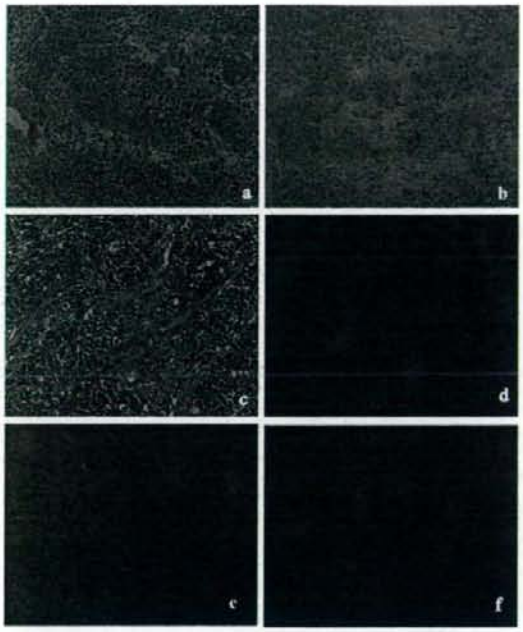

Figure 4. Expression of Egr-2, a marker of early Schwann cell differentiation, in human NB tumors and the xenografted NB tumors with hBMSCs. Cryosection of a differentiating NB tumor from a patient, showing Egr2-positive cells in the stroma (**a**, **b**). In xenografted NB tumors (**c**), Egr2-positive cells (blue) were observed (**d**) and these cells were also EGFP-positive (red) (**e** and **f**).

positive (Figure 4, c–f; and Supplemental Figure S3B, see *http://ajp.amjpathol.org*). These results support the proposal that inoculated hBMSCs differentiate into Schwann cells.

Contribution of hBMSCs to Blood Vessels and Other Tumor Stromal Components

Serial observations of NB tumors (SK-N-DZ) inoculated with hBMSCs showed that EGFP-positive hBMSCs formed blood vessel-like structures that contained red blood cells in their lumen (Figure 5a). We examined whether the EGFP-positive cells expressed certain endothelial markers (CD31, CD34, or CD105), or pericytic markers (α-smooth muscle actin), by immunohistochemically double-staining the cells with anti-GFP and anti-CD31, CD34, CD105, or α-smooth muscle actin. The EGFP-positive cells that formed vessel-like structures expressed only α-smooth muscle actin, and not CD31, CD34, or CD105 (Figure 5b). Thus, the EGFP-hBMSCs seem to function as pericytes, forming the lining of vessel walls in NB tumors. We observed a quantitative alteration in the stromal elements induced by the inoculation of hBMSCs into NB tumors. The stromal network of NB tumors inoculated with hBMSCs, which were immunostained using an α-smooth muscle actin antibody, was more widespread than that of NB tumors not inoculated with hBMSCs (Figure 5, c and d). Anti-α-smooth muscle

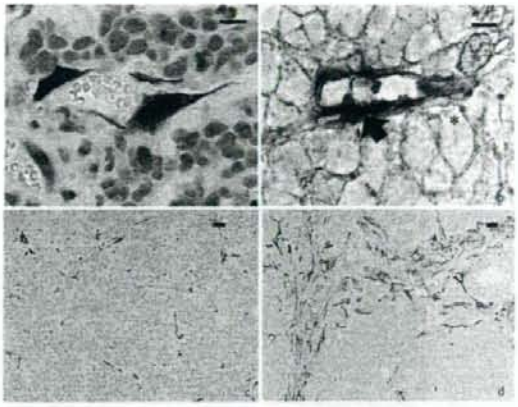

Figure 5. Contribution of hBMSCs to blood vessel and other tumor stromal components. **a:** EGFP-positive hBMSCs formed blood vessel-like structures containing red blood cells in NB tumors (SK-N-DZ) inoculated with hBMSCs. **b:** EGFP-positive cells (brown) that formed a vessel-like lumen expressed only α-smooth muscle actin (dark blue) by immunohistochemical double staining using GFP and α-smooth muscle actin antibodies (no nuclear staining using hematoxylin). **c:** The stromal network in a xenografted human NB tumor without hBMSC inoculation, immunostained with an α-smooth muscle actin antibody. The scattered distribution of α-smooth muscle actin-positive cells showed murine stromal elements because the α-smooth muscle actin antibody reacted with both murine and human α-smooth muscle actin. **d:** The stromal network in a xenografted human NB tumor inoculated with hBMSCs, immunostained with anti-α-smooth muscle actin antibody. More α-smooth muscle actin-positive cells are seen than in the NB tumor without hBMSC inoculation (**c**) and the area of α-smooth muscle actin-positive cells is wider. **Asterisk** shows NB cell; **arrow** indicates stromal cell). Scale bars: 50 μm (**a**, **b**); 20 μm (**c**, **d**).

actin reacts with both murine and human α-smooth muscle actin, so actin-positive cells (Figure 5c) were present in the murine stromal elements of the xenografted human NB tumors not inoculated with hBMSCs. However, many more α-smooth muscle actin-positive cells were seen in NB tumors inoculated with hBMSCs, and the area of the α-smooth muscle actin-positive cells was relatively more widespread because the α-smooth muscle actin-positive cells were large and more frequent (Figure 5d). The α-smooth muscle actin-positive cells were almost always immunohistochemically positive for GFP (Supplemental Figure S4, see *http://ajp.amjpathol.org*). These results indicate that the hBMSCs inoculated into NB tumors survived as a stromal component and were incorporated into blood vessel structures as pericytes and formed myofibroblasts.

Induction of S100beta in Stromal Cells by Co-Culture with NB Cells

We examined whether NB cells could induce the differentiation of hBMSCs or hMSCs into Schwann cells *in vitro*. We cultured hBMSCs or hMSCs with human NB cells (SK-N-DZ or SK-N-AS). We cultured stromal cells and NB cells with cell-to-cell contact, and stromal cells and NB cells using the transwell plates with micropores (0.4 μm), without cell-to-cell contact. The expression of S100beta, a Schwann cell-specific marker, was observed in cultures under both conditions. On the other hand, S100beta-positive cells were not observed in

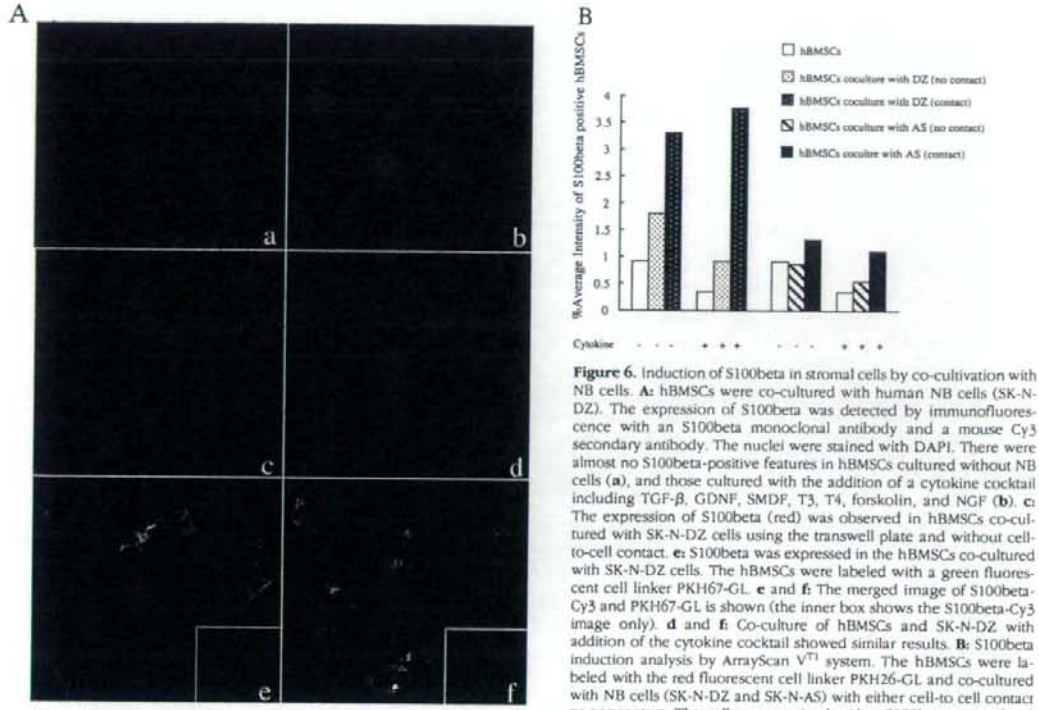

Figure 6. Induction of S100beta in stromal cells by co-cultivation with NB cells. **A:** hBMSCs were co-cultured with human NB cells (SK-N-DZ). The expression of S100beta was detected by immunofluorescence with an S100beta monoclonal antibody and a mouse Cy3 secondary antibody. The nuclei were stained with DAPI. There were almost no S100beta-positive features in hBMSCs cultured without NB cells (**a**), and those cultured with the addition of a cytokine cocktail including TGF-β, GDNF, SMDF, T3, T4, forskolin, and NGF (**b**). **c:** The expression of S100beta (red) was observed in hBMSCs co-cultured with SK-N-DZ cells using the transwell plate and without cell-to-cell contact. **e:** S100beta was expressed in the hBMSCs co-cultured with SK-N-DZ cells. The hBMSCs were labeled with a green fluorescent cell linker PKH67-GL. **e** and **f:** The merged image of S100beta-Cy3 and PKH67-GL is shown (the inner box shows the S100beta-Cy3 image only). **d** and **f:** Co-culture of hBMSCs and SK-N-DZ with addition of the cytokine cocktail showed similar results. **B:** S100beta induction analysis by ArrayScan V^{T1} system. The hBMSCs were labeled with the red fluorescent cell linker PKH26-GL and co-cultured with NB cells (SK-N-DZ and SK-N-AS) with either cell-to cell contact or noncontact. The cells were stained with a S100beta monoclonal antibody and a mouse FITC secondary antibody after the co-culture for 6 days. The percentage of S100beta FITC-positive hBMSCs in total hBMSCs labeled with red fluorescent linker PKH26-GL was estimated with or without the cytokine cocktail by the ArrayScan V^{T1} system.

hBMSCs cultured without NB cells (Figure 6Aa). Quantitative analysis using the ArrayScan V^{T1} system revealed significantly more induction of S100beta FITC fluorescence in hBMSCs when co-cultured with NB cells, both when there was or was not cell-to-cell contact with NB cells, compared with that in hBMSCs not co-cultured with NB cells. These results show that NB cells can induce the differentiation of stromal cells to Schwann cells *in vitro*. We found that a cytokine cocktail containing growth factors such as TGF-β, NGF, GDNF, SMDF, T3, T4, and forskolin,[18–22] did not affect the expression of S100beta in the presence or absence of NB cells (Figure 6).

Induction of Egr-2 in Stromal Cells by Co-Cultivation with NB Cells

We examined whether Egr-2, a transcription factor expressed during the early development of Schwann cells, was induced during the differentiation of hBMSCs or hMSCs to Schwann cells *in vitro*. The expression of Egr-2 was significantly elevated in hBMSCs or hMSCs co-cultured with NB cells, compared with hBMSCs or hMSCs not co-cultured with NB cells (Figure 7). Egr-2 expression was induced in stromal cells in co-cultures with SK-N-DZ or SK-N-AS cells. The expression of Egr-2 in the absence of NB cells was not affected by the addition of a cytokine cocktail containing the growth factors, TGF-β, NGF, GDNF, SMDF, T3, T4, and forskolin (Figure 7A). Furthermore, hMSCs were co-cultured with NB cells in the presence of TGF-β (10 μg/ml) because TGF-β was suspected to be involved in the tumor-stromal interactions that cause hMSCs to differentiate into Schwann cells.[24] However, the addition of TGF-β did not influence the expression of Egr-2 in the co-cultures (Figure 7B). The result of hBMSCs co-cultured with SK-N-AS or SK-N-DZ in the presence of TGF-β (or cytokine cocktail) was similar to that of hMSCs.

Induction of Egr-2 in Human Fibroblasts Cultivated with NB Cells

To test whether the differentiation of Schwann cells was specific to certain cell types, we examined whether human fibroblasts, MRC-5 (originating from human fetal lung tissue) and KMS-6 (originating from a whole human embryo), differentiated into Schwann cells in the presence of NB cells. MRC-5 or KMS-6 cells were co-cultured with NB cells (SK-N-DZ) using transwell plates and the expression of Egr-2 in the MRC-5 or KMS-6 cells was analyzed using immunoblotting. There was a slight increase in the expression of Egr-2 in the MRC-5 cells co-cultured with the SK-N-DZ cells, whereas there was no

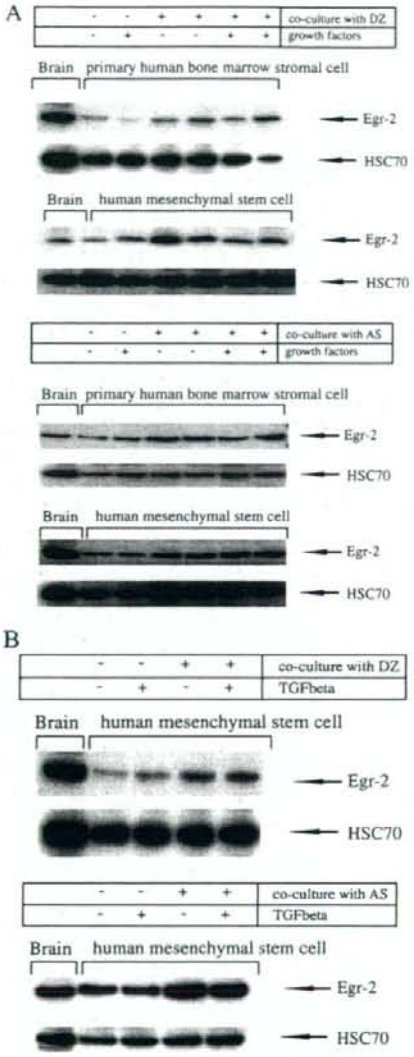

Figure 7A. Induction of Egr-2 in stromal cells by culture with NB cells. Co-culture of hBMSCs or hMSCs with human NB cells (SK-N-DZ and SK-N-AS) was without direct contact between hBMSCs or hMSCs and NB cells, using transwell plates with pores (pore size, 0.4 μm). There was increased expression of Egr-2 in hBMSCs or hMSCs co-cultured with NB cells compared with those without co-culture with NB cells. The addition of a cytokine cocktail including TGF-β, GDNF, SMDF, T3, T4, forskolin, and NGF did not alter the expression of Egr-2. Total cell lysates were examined by immunoblotting with a mouse anti-human Egr-2 antibody. Human brain tissue lysate was used as a positive control for Egr-2 protein. **B:** TGF-β did not induce Schwannian differentiation of hMSCs. HMSCs were co-cultured with SK-N-DZ and SK-N-AS cells with the addition of TGF-β (10 μg/ml) only and the Egr-2 expression in hMSCs was monitored by immunoblotting. There was no change in expression of Egr-2.

significant change in Egr-2 expression in the KMS-6 and HE-1 cells (Figure 8). These results suggest that human fibroblasts are a phenotypically heterogeneous cell population.

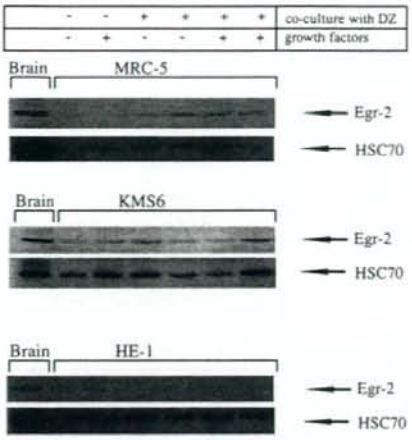

Figure 8. Induction of Egr-2 in human fibroblasts by culture with NB cells. Slightly increased expression of Egr-2 in MRC-5 cells was observed after co-culture with NB cells; no significant change was shown in KMS-6 and HE-1 cells after co-culture with NB cells.

Discussion

Tumor stroma is composed of a variety of cells and tissues, including fibroblasts, blood vessels, inflammatory cells, and extracellular matrices. Tumor-stroma interactions play critical roles in tumor cell growth, invasion, and metastasis through the control of signal transduction for cell proliferation, apoptosis, angiogenesis, and the augmentation of tumor cell motility and/or adhesion. A number of growth factors, angiogenic factors, and proteinases involved in tumor development are secreted, not only by tumor cells, but also by stromal cells.[25] The Schwannian stroma in NB tumors is a very specific stroma compared with other tumor stroma concerning differentiation and prognosis of NB tumors. Nevertheless, the origins of the cells composing tumor stroma remain uncertain. Raffi and colleagues,[11] using $ald1^{+/-}Id3^{-/-}$ mice model, reported that the tumor vessels and/or stroma are likely to be formed by the $Flk\text{-}1^{+}$ or $Flt\text{-}1^{+}$ fraction of bone marrow cells.[12] Myofibroblasts and fibroblasts in tumor stroma have also been reported to originate from bone marrow in a murine model for pancreatic tumors.[13]

Recently, anti-tumor therapy using mesenchymal stem cells has been tested in malignant tumors such as glioma, colon cancer, and Kaposi's sarcoma, based on the hypothesis that mesenchymal stem cells could constitute the tumor stroma.[25–38] These studies showed that tumor cell proliferation or tumor growth was impaired by the mesenchymal stem cells carrying therapeutic genes or molecules.

We have developed an animal model for human tumor-stroma research using human stromal cells derived from bone marrow. We found that the primary stromal cells or mesenchymal stem cells from human bone marrow may comprise the tumor stroma of xenografted human tumor, such as NB or Ewing's sarcoma, in murine subcutaneous tissues. This experimental model may be useful to study

in vivo interactions between neoplastic cells and stromal cells and for the advancement of tumor-stroma biology through histology, immunohistochemistry, or *in situ* hybridization techniques. Tumor stroma composed of hBMSCs or hMSCs may be functional in human xenografted tumors, because the inoculated hBMSCs or hMSCs developed into NB-specific Schwannian stroma and formed the lining of microvessels.

The size or weight of the xenografted NB tumors inoculated with hBMSCs and those without hBMSCs did not differ (data not shown). In the co-culture experiments, both apoptosis and proliferation of NB cells were augmented by their association with hBMSCs. Using flow cytometry, we observed an increased number of ssDNA-positive NB cells and an increased number of MIB-1 (Ki-67)-positive NB cells after co-culture with hBMSCs (Supplemental Figure S5, see *http://ajp.amjpathol.org*). These results show that the inoculation of hBMSCs into NB tumors may not have influenced tumor growth despite the accompanying Schwannian stroma formations.

The presence and volume of the Schwannian stroma is closely related with the prognosis of patients with NB. Schwannian stroma-rich/stroma-dominant NB tumors are associated with a more favorable outcome.[2] The development of Schwannian stroma is thought to be associated with the differentiation of NBs.[2] Ambros and colleagues[9] reported that neural differentiation was enhanced and the apoptotic rate was increased in NB cells co-cultivated with normal Schwann cells *in vitro*. Liu and colleagues[39] also reported that Schwann cells influenced proliferation, differentiation, and apoptosis of NB cells and angiogenesis in NB, using a murine sciatic nerve-engrafted NB xenograft model. Using cytogenetic procedures, Mora and colleagues[5] reported that Schwannian cells are derived from neoplastic NB cells. However, Ambros and colleagues[7] stated that the Schwann cells in NB tumors originated from nonneoplastic cells because the neoplastic NB cells showed aberrations in the number of chromosomes and the Schwann cells contained a normal number of chromosomes, when examined using fluorescence *in situ* hybridization. Liu and colleagues,[39] using the sciatic nerve-engrafted NB xenograft model, also concluded that the Schwann cells infiltrating into xenografted NB tumors were derived from the murine peripheral nerve tissues around the NB tumors, but not from the inoculated human NB cells. We only observed Schwann cells in NB tumors containing hBMSCs or hMSCs, which is compatible with the theory that the Schwannian stroma originates from nonneoplastic cells. In addition, we did not observe Schwann cells in xenografted human NB tumors that were not inoculated with hBMSCs or hMSCs. This may indicate that the factors produced by human NB cells cannot cause murine stromal cells to develop into stromal elements, such as microvessels. These observations do not necessarily mean that Schwannian stroma in patients with NBs originate from bone marrow cells. Cells such as fibroblasts that are recruited from neighboring tissues may constitute the tumor stroma because we observed that human fibroblasts (MRC-5 cells) differentiated into Schwann cells when co-cultured with SK-N-DZ cells.

Both of the two NB cell lines, SK-N-DZ and SK-N-AS, could induce Schwannian cell differentiation of hBMSCs *in vivo* and *in vitro*, but the differentiation of induction ability was observed. Two pathologists evaluated independently the volume of S100/S100beta-positive stroma in SK-N-DZ and SK-N-AS tumors by microscope. The evaluation showed that S100/S100beta-positive stroma in SK-N-DZ tumors with human stromal cells was more than that in SK-N-AS tumors (Supplemental Figure S3, a and b; see *http://ajp.amjpathol.org*). Furthermore, S100beta induction *in vitro* in hBMSCs by co-culture with SK-N-DZ cells was more effective than by SK-N-AS cells (Figure 6B). SK-N-DZ cells exhibit MYCN amplification of 30 times and SK-N-AS did not exhibit MYCN amplification. Retinoic acid has been reported to induce cellular differentiation in SK-N-DZ cells.[16] By contrast, retinoic acid is also reported to partially inhibit the proliferation of SK-N-AS cells and not to induce cellular differentiation.[17] The mechanism of differentiation and reactivity to induction differs between SK-N-DZ cells and SK-N-AS cells.

The hBMSCs and hMSCs differentiated into Schwann cells when they were co-cultured with NB cells using transwell plates. Humoral factors have been suggested to induce BMSCs and MSCs to differentiate into Schwann cells. Several humoral factors, including forskolin, NGF, SMDF, and T3, are reported to be related to Schwann cell differentiation.[22] However, we did not observe the differentiation of BMSCs or MSCs into Schwann cells after the addition of these humoral factors. The expression of the TGF-β receptor in Schwann cells and their progenitors has been documented, and the TGF-β signaling pathway is reported to be involved in Schwann cell development, myelination, proliferation, and apoptosis.[18,24] However, the addition of TGF-β did not significantly influence the differentiation of hBMSCs or hMSCs into Schwann cells in this study (the data for hBMSCs with TGF-β was not shown). It is possible that an unknown humoral factor(s) may be produced by the NB cells.

We used S100 as a marker of Schwannian stroma in the histological examination of the NBs, similar to the protocol used for the clinicopathological evaluation of NBs. However, S100 protein is always expressed in hBMSCs and hMSCs *in vitro* because of the existence of adipocytes among the hBMSCs and hMSCs. Thus, we used the Schwann cell-specific marker S100beta and NGFRp75 for increased precision. Egr-2 was also used to evaluate the early stage differentiation of Schwann cells. Egr-2 expression was monitored using immunoblotting during the Schwann cell differentiation of the hBMSCs and hMSCs co-cultured with NB cells. Several molecules including Egr-1, Egr-2, GAP-43, O4, MAG, and CNPase are expressed during Schwann cell differentiation.[23,40–42] Egr-2 is a transcription factor expressed in Schwann cell precursors during the early stages of differentiation, and the increased expression of Egr-2 is seen after nerve impairment.[23] Egr-2 is thought to be a marker for earl-stage cellular differentiation into Schwann cells.

We also examined whether other types of human cells, such as fibroblasts from human embryo, fetal lung or skin tissue, were also able to differentiate into Schwann cells

in NB tumors. MRC-5 cells (originating from human fetal lung tissue) were induced to differentiate into Schwann cells by co-culturing with NB cells SK-N-DZ, as seen with the hBMSCs. However, the KMS-6 cells (originating from a human embryo) and the HE-1 cells (originating from human skin) did not differentiate into Schwann cells. Thus, fibroblasts may represent a heterogeneous cell population. Differences in gene expression between the MRC-5, KMS-6, and HE-1 cells may explain the molecular mechanism responsible for the induction of Schwann cell differentiation. Egr-2 induction was only seen in the co-cultures of fibroblasts (MRC-5) and SK-N-DZ cells but not in the co-cultures of fibroblasts and SK-N-AS cells. This may be attributable to the difference in differentiation between the SK-N-DZ cells and the SK-N-AS cells. In this model, the hBMSCs contributed to the formation of microvessel structures such as pericytes or myofibroblasts. This phenomenon may be compatible with evidence showing that Flk-1$^+$ or Flt-1$^+$ cells from bone marrow are involved in tumor angiogenesis because some hBMSCs and hMSCs are known to express Flk-1and Flt-1.[11,12] The use of Schwann cells as a therapy for NB may be reasonable, but Schwann cells are hard to obtain. A useful source of Schwann cells may be hBMSCs and hMSCs because these cells have both proliferative capacity and multipotency.

We have presented an animal model for the reconstruction of human tumor stroma by injecting hBMSCs or mesenchymal stem cells into xenografted NB tumors. We have shown that stromal cells derived from bone marrow differentiate into Schwann cells in NB tumors *in vivo* and in co-culture with NB cells *in vitro*. These observations suggest that the origin of Schwannian stroma in NB tumors may be nonneoplastic cells rather than NB cells.

Acknowledgments

We thank Dr. Robert G. Hawley (American Red Cross, Washington, DC) for generously providing an expression vector of PG13/MSGFP, Dr. Akinori Hashiguchi for advice on expression vector construction, Ms. Maki Morioka-Iwata and Ms. Megumi Takamatsu for technical assistance, Mr. Hiroshi Suzuki for immunohistochemistry, and Ms. Tsukiko Hirabayashi for animal care.

References

1. Shimada H, Ambros IM, Dehner LP, Hata J, Joshi VV, Roald B: Terminology and morphologic criteria of neuroblastic tumors: recommendations by the International Neuroblastoma Pathology Committee. Cancer 1999, 86:349–363
2. Shimada H, Ambros IM, Dehner LP, Hata J, Joshi VV, Roald B, Stram DO, Gerbing RB, Lukens JN, Matthay KK, Castleberry RP: The International Neuroblastoma Pathology Classification (the Shimada system). Cancer 1999, 86:364–372
3. Ambros IM, Hata J, Joshi VV, Roald B, Dehner LP, Tuchler H, Potschger U, Shimada H: Morphologic features of neuroblastoma (Schwannian stroma-poor tumors) in clinically favorable and unfavorable groups. Cancer 2002, 94:1574–1583
4. Ikeda H, Iehara T, Tsuchida Y, Kaneko M, Hata J, Naito H, Iwafuchi M, Ohnuma N, Mugishima H, Toyoda Y, Hamazaki M, Mimaya J, Kondo S, Kawa K, Okada A, Hiyama E, Suita S, Takamatsu H: Experience with International Neuroblastoma Staging System and Pathology Classification. Br J Cancer 2002, 86:1110–1116
5. Mora J, Cheung NK, Juan G, Illei P, Cheung I, Akram M, Chi S, Ladanyi M, Cordon-Cardo C, Gerald WL: Neuroblastic and Schwannian stromal cells of neuroblastoma are derived from a tumoral progenitor cell. Cancer Res 2001, 61:6892–6898
6. Ambros IM, Ambros PF: Schwann cells in neuroblastoma. Eur J Cancer 1995, 31A:429–434
7. Ambros IM, Zellner A, Roald B, Amann G, Ladenstein R, Printz D, Gadner H, Ambros PF: Role of ploidy, chromosome 1p, and Schwann cells in the maturation of neuroblastoma. N Engl J Med 1996, 334:1505–1511
8. Katsetos CD, Karkavelas G, Frankfurter A, Vlachos IN, Vogeley K, Schober R, Wechsler W, Urich H: The stromal Schwann cell during maturation of peripheral neuroblastomas. Immunohistochemical observations with antibodies to the neuronal class III beta-tubulin isotype (beta III) and S-100 protein. Clin Neuropathol 1994, 13:171–180
9. Ambros IM, Attarbaschi A, Rumpler S, Luegmayr A, Turkof E, Gadner H, Ambros PF: Neuroblastoma cells provoke Schwann cell proliferation in vitro. Med Pediatr Oncol 2001, 36:163–168
10. Gregory CA, Prockop DJ, Spees JL: Non-hematopoietic bone marrow stem cells: molecular control of expansion and differentiation. Exp Cell Res 2005, 306:330–335
11. Lyden D, Young AZ, Zagzag D, Yan W, Gerald W, O'Reilly R, Bader BL, Hynes RO, Zhuang Y, Manova K, Benezra R: Id1 and Id3 are required for neurogenesis, angiogenesis and vascularization of tumour xenografts. Nature 1999, 401:670–677
12. Lyden D, Hattori K, Dias S, Costa C, Blaikie P, Butros L, Chadburn A, Heissig B, Marks W, Witte L, Wu Y, Hicklin D, Zhu Z, Hackett NR, Crystal RG, Moore MA, Hajjar KA, Manova K, Benezra R, Rafii S: Impaired recruitment of bone-marrow-derived endothelial and hematopoietic precursor cells blocks tumor angiogenesis and growth. Nat Med 2001, 7:1194–1201
13. Direkze NC, Hodivala-Dilke K, Jeffery R, Hunt T, Poulsom R, Oukrif D, Alison MR, Wright NA: Bone marrow contribution to tumor-associated myofibroblasts and fibroblasts. Cancer Res 2004, 64:8492–8495
14. Bhowmick NA, Chytil A, Plieth D, Gorska AE, Dumont N, Shappell S, Washington MK, Neilson EG, Moses HL: TGF-beta signaling in fibroblasts modulates the oncogenic potential of adjacent epithelia. Science 2004, 303:848–851
15. Pittenger MF, Mackay AM, Beck SC, Jaiswal RK, Douglas R, Mosca JD, Moorman MA, Simonetti DW, Craig S, Marshak DR: Multilineage potential of adult human mesenchymal stem cells. Science 1999, 284:143–147
16. Matsumoto M, Akiyama T, Miyatake S, Oda Y, Kikuchi H, Hanaoka M, Namba Y: Expression of proto-oncogene products during drug-induced differentiation of a neuroblastoma cell line SK-N-DZ. Acta Neuropathol (Berl) 1989, 79:217–221
17. Gaetano C, Matsumoto K, Thiele CJ: Retinoic acid negatively regulates p34cdc2 expression during human neuroblastoma differentiation. Cell Growth Differ 1991, 2:487–493
18. McLennan IS, Koishi K: The transforming growth factor-betas: multifaceted regulators of the development and maintenance of skeletal muscles, motoneurons and Schwann cells. Int J Dev Biol 2002, 46:559–567
19. Frostick SP, Yin Q, Kemp GJ: Schwann cells, neurotrophic factors, and peripheral nerve regeneration. Microsurgery 1998, 18:397–405
20. Leimeroth R, Lobsiger C, Lussi A, Taylor V, Suter U, Sommer L: Membrane-bound neuregulin1 type III actively promotes Schwann cell differentiation of multipotent Progenitor cells. Dev Biol 2002, 246:245–258
21. Mercier G, Turque N, Schumacher M: Rapid effects of triiodothyronine on immediate-early gene expression in Schwann cells. Glia 2001, 35:81–89
22. Sulairman OA, Gordon T: Transforming growth factor-beta and forskolin attenuate the adverse effects of long-term Schwann cell denervation on peripheral nerve regeneration in vivo. Glia 2002, 37:206–218
23. Topilko P, Levi G, Merlo G, Mantero S, Desmarquet C, Mancardi G, Charnay P: Differential regulation of the zinc finger genes Krox-20 and Krox-24 (Egr-1) suggests antagonistic roles in Schwann cells. J Neurosci Res 1997, 50:702–712
24. Unsicker K, Strelau J: Functions of transforming growth factor-beta isoforms in the nervous system. Cues based on localization and

experimental in vitro and in vivo evidence. Eur J Biochem 2000, 267:6972–6975
25. Liotta LA, Kohn EC: The microenvironment of the tumour-host interface. Nature 2001, 411:375–379
26. Loffek S, Zigrino P, Angel P, Anwald B, Krieg T, Mauch C: High invasive melanoma cells induce matrix metalloproteinase-1 synthesis in fibroblasts by interleukin-1alpha and basic fibroblast growth factor-mediated mechanisms. J Invest Dermatol 2005, 124:638–643
27. Tang Y, Nakada MT, Kesavan P, McCabe F, Millar H, Rafferty P, Bugelski P, Yan L: Extracellular matrix metalloproteinase inducer stimulates tumor angiogenesis by elevating vascular endothelial cell growth factor and matrix metalloproteinases. Cancer Res 2005, 65:3193–3199
28. Lang SH, Clarke NW, George NJ, Testa NG: Scatter factor influences the formation of prostate epithelial cell colonies on bone marrow stroma in vitro. Clin Exp Metastasis 1999, 17:333–340
29. Ikebe T, Nakayama H, Shinohara M, Shirasuna K: NF-kappaB involvement in tumor-stroma interaction of squamous cell carcinoma. Oral Oncol 2004, 40:1048–1056
30. St Croix B, Rago C, Velculescu V, Traverso G, Romans KE, Montgomery E, Lal A, Riggins GJ, Lengauer C, Vogelstein B, Kinzler KW: Genes expressed in human tumor endothelium. Science 2000, 289:1197–1202
31. Paweletz CP, Charboneau L, Bichsel VE, Simone NL, Chen T, Gillespie JW, Emmert-Buck MR, Roth MJ, Petricoin IE, Liotta LA: Reverse phase protein microarrays which capture disease progression show activation of pro-survival pathways at the cancer invasion front. Oncogene 2001, 20:1981–1989
32. Fox JM, Chamberlain G, Ashton BA, Middleton J: Recent advances into the understanding of mesenchymal stem cell trafficking. Br J Haematol 2007, 137:491–502
33. Nakamura K, Ito Y, Kawano Y, Kurozumi K, Kobune M, Tsuda H, Bizen A, Honmou O, Niitsu Y, Hamada H: Antitumor effect of genetically engineered mesenchymal stem cells in a rat glioma model. Gene Ther 2004, 11:1155–1164
34. Nakamizo A, Marini F, Amano T, Khan A, Studeny M, Gumin J, Chen J, Hentschel S, Vecil G, Dembinski J, Andreeff M, Lang FF: Human bone marrow-derived mesenchymal stem cells in the treatment of gliomas. Cancer Res 2005, 65:3307–3318
35. Hung SC, Deng WP, Yang WK, Liu RS, Lee CC, Su TC, Lin RJ, Yang DM, Chang CW, Chen WH, Wei HJ, Gelovani JG: Mesenchymal stem cell targeting of microscopic tumors and tumor stroma development monitored by noninvasive in vivo positron emission tomography imaging. Clin Cancer Res 2005, 11:7749–7756
36. Komarova S, Kawakami Y, Stoff-Khalili MA, Curiel DT, Pereboeva L: Mesenchymal progenitor cells as cellular vehicles for delivery of oncolytic adenoviruses. Mol Cancer Ther 2006, 5:755–766
37. Khakoo AY, Pati S, Anderson SA, Reid W, Elshal MF, Rovira, II, Nguyen AT, Malide D, Combs CA, Hall G, Zhang J, Raffeld M, Rogers TB, Stetler-Stevenson W, Frank JA, Reitz M, Finkel T: Human mesenchymal stem cells exert potent antitumorigenic effects in a model of Kaposi's sarcoma. J Exp Med 2006, 203:1235–1247
38. Studeny M, Marini FC, Champlin RE, Zompetta C, Fidler IJ, Andreeff M: Bone marrow-derived mesenchymal stem cells as vehicles for interferon-beta delivery into tumors. Cancer Res 2002, 62:3603–3608
39. Liu S, Tian Y, Chlenski A, Yang Q, Zage P, Salwen HR, Crawford SE, Cohn SL: Cross-talk between Schwann cells and neuroblasts influences the biology of neuroblastoma xenografts. Am J Pathol 2005, 166:891–900
40. Trejo O, Reed JA, Prieto VG: Atypical cells in human cutaneous re-excision scars for melanoma express p75NGFR, C56/N-CAM and GAP-43: evidence of early Schwann cell differentiation. J Cutan Pathol 2002, 29:397–406
41. Mirsky R, Parkinson DB, Dong Z, Meier C, Calle E, Brennan A, Topilko P, Harris BS, Stewart HJ, Jessen KR: Regulation of genes involved in Schwann cell development and differentiation. Prog Brain Res 2001, 132:3–11
42. Sprinkle TJ, Agee JF, Tippins RB, Chamberlain CR, Faguet GB, De Vries GH: Monoclonal antibody production to human and bovine 2':3'-cyclic nucleotide 3'-phosphodiesterase (CNPase): high-specificity recognition in whole brain acetone powders and conservation of sequence between CNP1 and CNP2. Brain Res 1987, 426:349–357

Original article

Aurora kinase B is a predictive factor for the aggressive recurrence of hepatocellular carcinoma after curative hepatectomy

S. Tanaka[1,2], S. Arii[2], M. Yasen[1,2], K. Mogushi[1], N. T. Su[4], C. Zhao[5], I. Imoto[5], Y. Eishi[3], J. Inazawa[5], Y. Miki[4] and H. Tanaka[1]

[1]Information Centre for Medical Sciences, [2]Department of Hepato-biliary-pancreatic Surgery and [3]Department of Pathology, Graduate School of Medicine, and Departments of [4]Molecular Genetics and [5]Molecular Cytogenetics, Medical Research Institute, Tokyo Medical and Dental University, Tokyo, Japan

Correspondence to: Dr S. Tanaka, Department of Hepato-biliary-pancreatic Surgery, Tokyo Medical and Dental University, Graduate School of Medicine, 1-5-45 Yushima, Bunkyo-ku, Tokyo 113-8519, Japan (e-mail: shinji.tnsrg@tmd.ac.jp)

Background: Patterns of cancer recurrence hold the key to prognosis after curative resection. This retrospective study aimed to identify a predictor and therapeutic candidate for aggressive recurrence of hepatocellular carcinoma (HCC).

Methods: Primary HCC tissues from 107 patients who had curative resection were analysed. Genome-wide gene expression profiles were investigated using a microarray technique, and clustering analysis was carried out based on the first diagnosis of recurrence according to the Milan criteria. Immunohistochemical expression and array-based comparative genomic hybridization (array-CGH) were also assessed.

Results: Microarray analysis revealed overexpression of Aurora kinase B, a chromosome passenger protein kinase, as the most significant predictor of the aggressive recurrence of HCC. Aurora kinase B protein expression was significantly associated with aggressive recurrence ($P < 0{\cdot}001$) and prognosis ($P < 0{\cdot}001$). Multivariable analysis identified Aurora kinase B as the only independent predictor of aggressive recurrence of HCC ($P = 0{\cdot}031$). Array-CGH analysis showed that genomic instability was closely related to Aurora kinase B expression ($P = 0{\cdot}011$).

Conclusion: Aurora kinase B is an effective predictor of aggressive HCC recurrence, in relation to the genomic instability. It might be worth considering as a molecular target for the adjuvant therapy of HCC.

Paper accepted 30 January 2008
Published online 29 February 2008 in Wiley InterScience (www.bjs.co.uk). **DOI:** 10.1002/bjs.6011

Introduction

Hepatocellular carcinoma (HCC) is a common fatal malignancy worldwide[1]. A major obstacle in its treatment is the high frequency of tumour recurrence even after curative resection. Indeed, the pattern of recurrence, rather than the recurrence itself, has critical effects on prognosis[2]. Prognosis has been shown to be closely associated with the pattern of recurrence of HCC defined according to the Milan criteria (solitary lesion of maximum diameter 5 cm, or up to three nodules of maximum diameter 3 cm, without major vascular invasion or distant metastasis)[3], which have been proposed for selection of patients with HCC for liver transplantation[4]. Even in the event of recurrence after curative resection, patients who meet these criteria have a good prognosis[3]. In contrast, when the recurrence exceeds the Milan criteria, treatment is limited and the prognosis poor[5].

In recent years, various molecules have been proposed as predictive markers for recurrence of HCC, but none has proved useful clinically because different patterns of recurrence were not considered[6,7]. The identification of novel biomarkers is required for the accurate prediction

The Editors are satisfied that all authors have contributed significantly to this publication

of aggressive recurrence at the first diagnosis of recurrent HCC[3].

Genome-wide gene expression analysis by microarray offers a systematic approach to gaining comprehensive information regarding transcription profiles[8]. Such studies have the potential to lead to the development of a novel molecular-targeted therapy for HCC[9]. The authors have previously analysed gene expression in HCC[10,11], and have identified novel molecules that might represent therapeutic targets[10,12]. The aim of the present study was to identify a marker associated with aggressive recurrence of HCC within 2 years of curative resection, by examination of the genome-wide expression profile of HCC generated by microarray study. The genes identified by such a comprehensive genetic analysis may shed light on the biological tumour characteristics that lead to recurrence, which might enable the development of a specific adjuvant therapy for HCC.

Methods

One hundred and seven patients underwent curative hepatectomy for HCC between 2000 and 2004 at Tokyo Medical and Dental University Hospital. Written informed consent was obtained from these patients, and the institutional review board approved the study. Forty patients were randomly assigned to a microarray training set, and the remaining 67 to a validation set. Resected tissues containing no necrosis were divided into two specimens immediately after surgery; one was snap-frozen in liquid nitrogen and stored at $-80°C$ for microarray analysis, and the other was fixed in 10 per cent formaldehyde solution and embedded in paraffin for histopathological analysis.

Patients were followed up with assays of serum level of α-fetoprotein and protein induced by vitamin K absence or antagonists II every month, and by ultrasonography, computed tomography (CT) and magnetic resonance imaging every 3 months. The mean observation time was 4·1 years. When tumour recurrence was suspected, precise diagnostic imaging was performed by means of CT angiography. Finally, the exact diagnosis of recurrence was made by imaging, and the number and size of the tumour(s) determined. At the first diagnosis of a recurrence within 2 years after the initial operation, the pattern was defined in accordance with the Milan criteria. A comparison of the characteristics of patients in the microarray and validation groups showed no statistically significant differences in clinicopathological features. No recurrence, recurrence meeting the Milan criteria and recurrence exceeding the criteria were noted in 18, nine and 13 patients respectively in the microarray group, compared with 32, 13 and 22 patients in the validation group ($P = 0·924$).

RNA preparation and microarray hybridization

Forty primary HCC specimens were obtained from the surgically resected materials. Total RNA was extracted from the sliced tissue specimens using an RNeasy kit (Qiagen, Hilden, Germany). The integrity of the RNA obtained was assessed using an Agilent 2100 BioAnalyzer (Agilent Technologies, Palo Alto, California, USA). For the gene expression analysis, 29 samples with an RNA integrity number greater than 5·0 were further analysed. There were no statistically significant differences in the clinicopathological features between the 29 samples analysed and the 11 discarded; no recurrence, recurrence meeting the criteria and recurrence exceeding the criteria were observed in 13, six and ten samples analysed respectively, compared with five, three and three discarded ($P = 0·869$). The rate of cancer cells was above 40 per cent (mean 81·0 per cent) in all 29 samples. Contaminating DNA was removed by digestion with RNase-free DNase (Qiagen). Complementary RNA was prepared from 2 μg total RNA, using one-cycle target labelling and a control reagents kit (Affymetrix, Santa Clara, California, USA). Hybridization and signal detection of the Human Genome U133 Plus 2.0 arrays (Affymetrix) were performed in accordance with the manufacturer's instructions.

Analysis of gene expression data

A total of 29 microarray data sets was normalized using the robust multiarray average method[13] with R 2.3.1 statistical software together with a BioConductor package[14]. The estimated gene expression levels were $\log_2$-transformed, and 62 control probe sets were removed for further analysis. For each 54 613 probes on the Human Genome U133 Plus 2.0 arrays, the fold change (FC) values were calculated using the ratio of the geometric means of the gene expression levels between the two groups. A Wilcoxon rank sum test was performed to estimate the significance levels of the differences in gene expression between them. Genes were selected for which both the $\log_2$(FC) values were greater than 1 (equivalent to FC more than 2·0 or FC less than 0·5; denoted FC > 2·0 for simplicity) and $P < 0·0002$ in the Wilcoxon rank sum test. A hierarchical clustering with the selected genes was performed with R software using the Euclidean distance and complete linkage method. For clustering, the expression data were standardized as z-scores (mean = 0 and variance = 1) for each probe.

Immunohistochemical analysis

To validate further the expression patterns detected by the microarray, immunohistochemical studies were performed on 22 HCC samples in the microarray group and an additional 67 HCC samples for validation. The primary antibody (Novus Biologicals, Littleton, Colorado, USA) was used at 1 : 50 dilution with phosphate-buffered saline containing 1 per cent bovine serum albumin. The tissue sections were stained with an automated immunostainer (BenchMark® XT; Ventana Medical Systems, Tucson, Arizona, USA) using heat-induced epitope retrieval and a standard diaminobenzidine detection kit (Ventana). Strong, diffuse, nuclear staining in more than 10 per cent of the cells was considered a positive result. Immunohistochemical staining was evaluated under a light microscope by two independent investigators.

Analysis of array-based comparative genomic hybridization and altered fraction of genome

The in-house array MCG Cancer Array-800, which contains 800 bacterial artificial chromosome/P1-derived artificial chromosome clones carrying genes or sequence-tagged site markers of potential importance in cancer genesis or progression, was used for array-based comparative genomic hybridization (array-CGH) analysis[15]. The hybridizations were carried out as described elsewhere[16] with minor modifications, using a HYBRIMASTER® HS-300eTAC hybridization machine (Aloka, Tokyo, Japan). The hybridized slides were scanned with GenePix 4000B (Axon Instruments, Foster City, California, USA) and the acquired images were analysed with GenePix Pro 6.0 imaging software (Axon Instruments). The fluorescence ratios were normalized so that the mean of the middle third of $\log_2$ ratios across the array was zero. Based on a previous control study[15], the thresholds for copy-number gain and loss were set at $\log_2$ ratios of 0·4 and $-0{\cdot}4$ respectively; $\log_2$ ratios greater than 2·0 were defined as high-level amplifications and $\log_2$ ratios below $-2{\cdot}0$ as homozygous deletions. To evaluate the genomic instability of each of the HCC tumours, the fraction of genome altered (FGA) was calculated based on the array-CGH data as described by Veltman and colleagues[17]. The FGA for each tumour was quantitated by assigning for each clone a distance equal to the sum of one half of the distance between its own centre and that of its neighbouring clones.

Statistical analysis

Statistical comparisons of clinicopathological characteristics were made using the χ^2 test or Fisher's exact test with a single degree of freedom, and Student's t test was used to analyse differences between continuous values. Cumulative patient survival rates were determined using the Kaplan–Meier method, and compared by means of the log rank test. $P < 0{\cdot}050$ was considered statistically significant.

To investigate the factors that predicted aggressive recurrence, multivariable analysis was performed using a logistic regression model. The following six factors were considered: expression of Aurora kinase B protein (no *versus* yes), the number of tumours (one or two *versus* three or more), tumour size (at least 5 cm *versus* less than 5 cm), portal vein invasion (no *versus* yes), hepatic vein invasion (no *versus* yes) and tumour node metastasis (TNM) stage (I/II/III *versus* IV). To select a set of factors that were strongly associated with aggressive recurrence, a stepwise variable selection was performed using the six factors. The initial model contained all six factors, and at each step a variable that minimized Akaike's information criterion was added or removed until convergence was achieved.

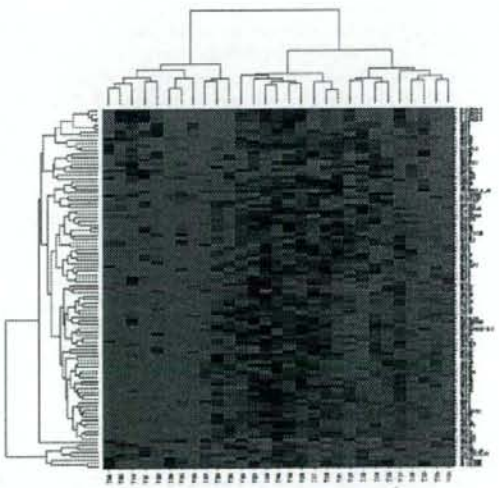

Fig. 1 Hierarchical clustering of primary hepatocellular carcinoma with recurrence exceeding the Milan criteria using probes satisfying both fold change (FC) > 2 and $P < 0{\cdot}0002$. T02, T04, T05, T08, T10, T11, T15, T27, T33 and T37 are the patients with aggressive recurrence (shown in red text). Red represents upregulation in the group with recurrence, and green downregulation in the others

a Levels of expression of Aurora kinase B protein

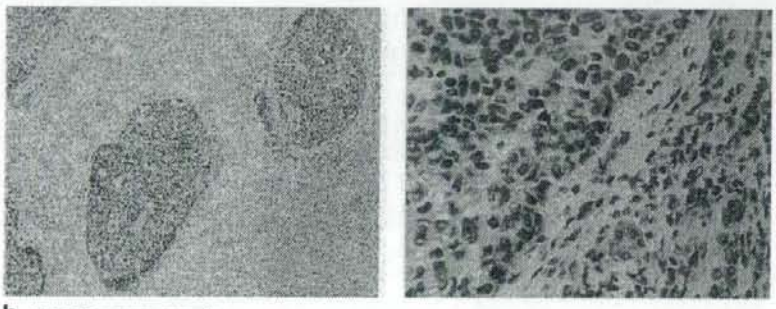

b Transition zone capsule

Fig. 2 Immunohistochemical analysis of Aurora kinase B in hepatocellular carcinoma (HCC) tissues. **a** HCC tissues showing negative (less than 10 per cent; left panel), moderate (10–20 per cent; middle panel) and strong (more than 20 per cent; right panel) staining intensities of Aurora kinase B protein in the nucleus of cancer cells, but not in the adjacent non-cancerous cells (original magnification ×100). **b** The transition zone capsule invading HCC cancer cells with Aurora kinase B expression at low magnification (×20; left panel) and high magnification (×400; right panel)

Results

Aurora kinase B as a predictor of aggressive recurrence of hepatocellular carcinoma

A gene expression analysis was performed for the 29 samples in the microarray test group in relation to aggressive recurrence. Among 54 613 probes, 101 that satisfied FC > 2·0 and Wilcoxon $P < 0{\cdot}0002$ were identified as differently expressed genes. *Fig. 1* shows the hierarchical clustering of the 101 probes. The patient numbers in red on the right denote patients with aggressive recurrence, indicating that the genes were divided into two clusters. As shown in *Table 1* and *Appendix 1* (available as supplementary material online; http://www.bjs.co.uk), it is of interest that the genes associated with cytokinesis (Aurora kinase B; switching/sucrose non-fermenting-related, matrix-associated, actin-dependent regulator of chromatin, subfamily c, member 1; minichromosome maintenance-deficient 2, mitotin (*Saccharomyces cerevisiae*); protein regulator of cytokinesis 1; microtubule-associated, homologue (*Xenopus laevis*); discs, large homologue 7 (*Drosophila*); citron (rho-interacting, serine/threonine kinase 21); and chromosome segregation 1-like) were highly upregulated in the primary HCC of patients who had aggressive recurrence exceeding the Milan criteria. Aurora kinase B, a chromosome passenger protein kinase, was potentially the strongest predictor of aggressive recurrence.

Aurora kinase B protein is overexpressed in HCC tissues in association with aggressive recurrence

To validate further the expression of Aurora kinase B as detected by microarray, immunohistochemical studies were performed on HCC tissues using Aurora kinase B antibody. Strong, diffuse, nuclear staining in more than 10 per cent of the cells, considered a positive result, was observed in tumour tissues, but not in adjacent normal liver tissue (*Fig. 2*). Aurora kinase B protein was detected in nine of 22 samples in the microarray test group. The microarray intensity of the Aurora kinase B gene was

Table 1 List of genes differently expressed in cases of recurrence exceeding the Milan criteria ($P < 0{\cdot}00003$)

No.	Probe ID	Gene symbol	Title	P	Fold change
1	209464_at	AURKB	Aurora kinase B	0·0000002	3·59
2	202503_s_at	KIAA0101	KIAA0101	0·0000007	5·24
3	201075_s_at	SMARCC1	Switching/sucrose non-fermenting (SWI/SNF)-related, matrix-associated, actin-dependent regulator of chromatin, subfamily c, member 1	0·0000012	2·46
4	202107_s_at	MCM2	MCM2, minichromosome maintenance-deficient 2, mitotin (*Saccharomyces cerevisiae*)	0·0000012	4·33
5	218009_s_at	PRC1	Protein regulator of cytokinesis 1	0·0000012	4·83
6	210052_s_at	TPX2	TPX2, microtubule-associated, homologue (*Xenopus laevis*)	0·0000019	3·92
7	203764_at	DLG7	Discs, large homologue 7 (*Drosophila*)	0·0000030	4·04
8	212801_at	CIT	Citron (rho-interacting, serine/threonine kinase 21)	0·0000030	2·56
9	218355_at	KIF4A	Kinesin family member 4A	0·0000030	4·11
10	201112_s_at	CSE1L	CSE1, chromosome segregation 1-like (yeast)	0·0000045	2·13
11	218755_at	KIF20A	Kinesin family member 20A	0·0000045	4·52
12	202705_at	CCNB2	Cyclin B2	0·0000097	3·22
13	204709_s_at	KIF23	Kinesin family member 23	0·0000097	3·07
14	206102_at	PSF1	DNA replication complex GINS protein PSF1	0·0000097	4·57
15	209642_at	BUB1	BUB1, budding uninhibited by benzimidazoles 1 homologue (yeast)	0·0000097	3·87
16	225687_at	C20orf129	Chromosome 20 open reading frame 129	0·0000097	4·52
17	1552619_a_at	ANLN	Anillin, actin-binding protein (scraps homologue, *Drosophila*)	0·0000097	3·38
18	202326_at	EHMT2	Euchromatic histone-lysine *N*-methyltransferase 2	0·0000139	2·14
19	206550_s_at	NUP155	Nucleoporin 155 kDa	0·0000139	2·49
20	210115_at	RPL39L	Ribosomal protein L39-like	0·0000139	2·55
21	226980_at	DEPDC1B	DEP domain-containing 1B	0·0000139	3·53
22	201111_at	CSE1L	CSE1 chromosome segregation 1-like (yeast)	0·0000194	2·26
23	201292_at	TOP2A	Topoisomerase (DNA) II alpha 170 kDa	0·0000194	5·22
24	204603_at	EXO1	Exonuclease 1	0·0000194	2·21
25	223271_s_at	CTDSPL2	CTD (carboxy-terminal domain, RNA polymerase II, polypeptide A) small phosphatase-like 2	0·0000194	2·07
26	201663_s_at	SMC4L1	SMC4 structural maintenance of chromosomes 4-like 1 (yeast)	0·0000269	2·89
27	207828_s_at	CENPF	Centromere protein F, 350/400 kDa (mitosin)	0·0000269	3·75
28	209714_s_at	CDKN3	Cyclin-dependent kinase inhibitor 3 (CDK2-associated dual-specificity phosphatase)	0·0000269	4·55
29	212639_x_at	K-ALPHA-1	Tubulin, alpha, ubiquitous	0·0000269	2·14
30	214710_s_at	CCNB1	Cyclin B1	0·0000269	4·21
31	223699_at	CNDP1	Carnosine dipeptidase 1 (metallopeptidase M20 family)	0·0000269	0·21
32	224753_at	CDCA5	Cell division cycle-associated 5	0·0000269	2·74
33	1555278_a_at	CKAP5	Cytoskeleton-associated protein 5	0·0000269	2·03

significantly higher in these nine samples than in the remaining 13 (FC = 2·3; $P = 0{\cdot}004$). The results of the immunohistochemical analysis confirmed the microarray findings at the protein expression level.

An additional 67 samples in the validation set were analysed. Again, nuclear staining in more than 10 per cent of the cells was noted in tumour tissue, but not in the adjacent normal liver. Immunohistochemical expression of Aurora kinase B was detected in 17 of 22 cases with aggressive recurrence, but in only eight of 45 without such recurrence ($P < 0{\cdot}001$). A close relationship between Aurora kinase B expression in the primary HCC and aggressive recurrence was confirmed.

The association between Aurora kinase B protein expression and other clinicopathological variables was investigated in the 67 patients (*Table 2*). There was a statistically significant relationship between Aurora kinase B protein expression and primary tumour number, tumour size, portal vein invasion, hepatic vein invasion and TNM stage.

Fig. 3 shows the survival rates after curative surgery of the 25 patients who were positive and the 42 who were negative for Aurora kinase B expression. The 5-year survival rate of the latter group was significantly higher (79 *versus* 24 per cent; $P < 0{\cdot}001$).

Multivariable analysis of aggressive recurrence and the significance of Aurora kinase B expression

Multivariable logistic regression of aggressive recurrence was performed using five clinicopathological factors and the immunohistological data (*Table 3*). The stepwise variable selection led to a model with three factors: tumour size, portal vein invasion and Aurora kinase B expression. The expression of Aurora kinase B was the only significant